Received: 12 May 2026 | Revised: 5 June 2026 | Accepted: 11 June 2026

DOI: 10.1002/suco.70697

fib CEB-FIP WILEY

ARTICLE

Flexural performance and design assessment of sustainable crumb rubber concrete beams reinforced with basalt-FRP bars

Yahia M. S. Ali[1,2,3] | Xin Wang[1,2] | Zhishen Wu[1,2] | Essam Jnead[4]

[1]Key Laboratory of C & PC Structures Ministry of Education, Southeast University, Nanjing, China

[2]National and Local Unified Engineering Research Center for Basalt Fiber Production and Application Technology, International Institute for Urban Systems Engineering, Southeast University, Nanjing, China

[3]Department of Civil Engineering, Faculty of Engineering, Assiut University, Assiut, Egypt

[4]School of Civil, Mining, and Environmental Engineering, University of Wollongong, Wollongong, New South Wales, Australia

Correspondence

Yahia M. S. Ali, Key Laboratory of C & PC Structures Ministry of Education, Southeast University, Nanjing 211189, China.

Email: yahiaali@seu.edu.cn

Funding information

The International Science & Technology Cooperation Program of China, Grant/Award Number: 2024YFE0198400; National Natural Science Foundation of China, Grant/Award Number: 52278244; Fundamental Research Funds for the Central Universities, Grant/Award Number: 2242024 k30039, 2242024 k30050

Abstract

Crumb rubber concrete (CRC) offers an environmentally sustainable solution for recycling waste tires through their use as a partial replacement for natural aggregates. However, limited research has investigated the structural behavior of CRC beams reinforced with basalt fiber-reinforced polymer (BFRP) bars. This study experimentally evaluates the flexural performance of CRC beams reinforced with BFRP bars under four-point bending. Fifteen reinforced concrete beams were tested to investigate the effects of crumb rubber (CR) replacement ratio (0%–20%), rubber particle size (5 mm and No. 20), reinforcement type (steel and BFRP), and BFRP reinforcement ratio on cracking behavior, stiffness, load-carrying capacity, and failure mode. The results showed that increasing CR content reduced concrete density, compressive strength, flexural strength, cracking load, stiffness, and ultimate load, with the reduction becoming more pronounced when finer rubber particles were used. CRC beams exhibited more distributed cracking patterns and greater deformation capacity than conventional concrete beams. Regardless of concrete type, BFRP-reinforced beams developed significantly higher ultimate loads than steel-reinforced beams due to the superior tensile strength of BFRP bars. Increasing the BFRP reinforcement ratio improved cracking resistance, post-cracking stiffness, and ultimate flexural capacity. Among the investigated mixtures, CRC containing 5% replacement of 5 mm CR exhibited the most favorable balance between sustainability and structural performance. Analytical predictions based on ACI 440.1R, CSA S806, AASHTO LRFD, Gb 50608, JSCE, SP295, and Eurocode-based formulations showed reasonable agreement with the experimental results. The findings demonstrate the feasibility of utilizing BFRP-reinforced CRC members as sustainable, lightweight, and corrosion-resistant structural elements for future infrastructure applications.

KEYWORDS

crumb rubber concrete, ductility, flexural behavior, FRP bars, waste tyre rubber

1 | INTRODUCTION

The disposal of scrap tires has become a significant environmental challenge due to the massive volume of waste generated by vehicular use. Millions of end-of-life tires are discarded in landfills each year, where their non-biodegradable nature fosters pest and mosquito proliferation.[1,2] To mitigate these issues, modern recycling methods must be adopted to reduce landfill dependence without causing ecological harm.[3] One promising approach is the partial replacement of mineral aggregates in concrete with recycled rubber, producing crumb rubber concrete (CRC).[4–6] This method not only conserves natural resources by reducing aggregate demand but also decreases the volume of rubber waste entering landfills.[7,8] Extensive research on CRC has consistently demonstrated that partial replacement of conventional aggregates with rubber particles leads to reductions in compressive strength, tensile strength, and modulus of elasticity compared to conventional concrete.[9–13] This reduction is primarily attributed to the poor adhesion between rubber particles and the cement matrix.[14–16] Despite these limitations, CRC offers distinct advantages over conventional concrete, including lower unit weight due to the reduced density of rubber compared to fine aggregates and enhanced energy absorption capacity.[17] Moreover, a significant improvement was demonstrated in ductility, toughness, impact resistance, energy dissipation, and damping ratio.[17–22] Many studies have demonstrated that CRC can achieve compressive strengths of 30–45 MPa, making it viable for structural use.[15,23,24] Recent studies have further emphasized the importance of sustainable and modified cementitious composites, including rubber/PET-modified concrete, fiber-reinforced concrete-filled steel tubes, nylon aggregate concrete, geopolymer concrete, and data-driven prediction models for concrete properties, demonstrating the growing interest in improving the mechanical, thermal, and durability performance of advanced concrete materials.[25–29]

To facilitate the adoption of CRC in structural elements such as beams and columns, a thorough understanding of its behavior under structural loads is essential. While limited studies exist on reinforced CRC beams, some findings indicate improved cracking resistance compared to conventional concrete.[30] Another study evaluated the flexural and shear capacity of reinforced CRC beams and suggested that existing design guidelines and shear models can predict shear capacity.[31] However, this study was limited to a single CRC mix, leaving the effect of rubber content on shear behavior unexplored. Previous research on rubberized concrete has primarily focused on material properties, with limited studies examining its structural behavior.[25–29] Son et al.[32] experimentally investigated the influence of waste tire rubber as a partial replacement of natural aggregate on the mechanical and flexural behavior of reinforced concrete members. Their study evaluated different rubber replacement ratios and examined the resulting changes in compressive strength, stiffness, cracking behavior, and load-carrying capacity. The results indicated that incorporating waste tire rubber generally reduced concrete strength and stiffness due to the lower rigidity and weaker interfacial bonding of rubber particles compared with conventional aggregates. However, the rubberized concrete specimens exhibited enhanced deformability, improved energy absorption capacity, and more distributed cracking patterns, demonstrating the potential of waste tire rubber for developing sustainable and ductile concrete composites. Ganesan et al.[30] studied rubberized beam-column joints under monotonic and cyclic loads, replacing 15% of fine aggregate volume with shredded rubber. The results revealed improved energy dissipation, ultimate deflection, and ductility but noted a reduction in load-bearing capacity. Al-Tayeb et al.[33] tested rubberized beams using 1.0 mm rubber with 5%–20% sand replacement. It was found that the bending capacity declined with higher rubber content.

Fiber-reinforced polymer (FRP) bars have gained prominence as a corrosion-resistant alternative to traditional steel reinforcement, addressing the costly maintenance issues associated with steel corrosion in reinforced concrete structures.[34] FRP reinforcements offer several distinct advantages, including a high strength-to-weight ratio, linear elastic behavior until failure, and superior tensile strength, though their lower elastic modulus results in reduced stiffness compared to steel-reinforced concrete (RC) beams.[35] The most commonly used FRP types—carbon-FRP (CFRP), glass-FRP (GFRP), and aramid-FRP (AFRP)—have been extensively studied and incorporated into design codes such as ACI 440.1R,[36] and CSA S806.[37] Recently, Basalt-FRP (BFRP) has emerged as a high-performance and sustainable alternative to conventional steel reinforcement, offering distinct advantages in both economic and structural performance.[38] Derived from molten basalt rock, BFRP exhibits higher tensile strength than steel while being 90% lighter, offering an exceptional strength-to-weight ratio.[39,40] However, BFRP-RC beams demonstrated higher ultimate load-carrying capacity and enhanced corrosion resistance compared with steel-RC beams; nevertheless, they exhibited lower ductility and wider crack widths due to the linear-elastic behavior and lower elastic modulus of

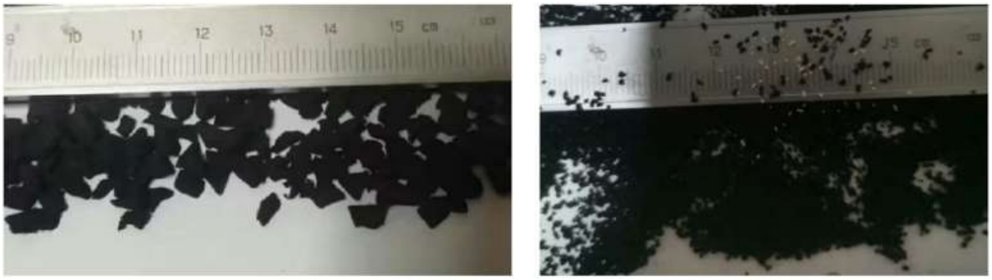

(a) (b)

FIGURE 1 Crumb rubber (CR) aggregate: (a) CR 5 mm; (b) CR No. 20.

BFRP bars.[41] Ali et al.[42] experimentally investigated the bond–slip behavior and failure mechanisms of BFRP bars embedded in CRC, focusing on the effects of rubber content, particle size, bar diameter, and surface treatment. The results demonstrated that a small rubber replacement ratio (5% with 5 mm particles) can enhance both compressive and bond strength, while higher rubber contents and finer particles significantly deteriorate mechanical and bond performance due to weak interfacial bonding. Among the reinforcement types, helically wounded BFRP bars exhibited the best bond performance, outperforming both sand-coated and wrapped bars, due to superior mechanical interlock. The bond–slip response of CRC was found to be similar to that of normal concrete, indicating its structural feasibility, although BFRP bars showed greater slip and more ductile behavior compared to steel.

Although several previous studies have investigated the mechanical properties of CRC and the structural performance of FRP-RC members independently, limited research has addressed the combined behavior of CRC beams reinforced with BFRP bars under flexural loading. In particular, the influence of CR particle size, replacement ratio, and BFRP reinforcement ratio on cracking behavior, stiffness degradation, ductility, strain response, and load-carrying capacity has not been comprehensively evaluated. Furthermore, the applicability of existing international FRP design provisions for predicting the flexural behavior of BFRP-reinforced CRC beams remains insufficiently understood. Therefore, the present study aims to experimentally investigate the flexural performance of CRC beams reinforced with BFRP bars under four-point bending. The effects of reinforcement type, reinforcement ratio, CR content, and rubber particle size are systematically examined. In addition, the experimental results are compared with several international design approaches to assess the accuracy and applicability of current FRP design provisions for sustainable CRC structural members. The outcomes of this study contribute to the development of environmentally sustainable and corrosion-resistant concrete structural systems.

2 | EXPERIMENTAL PROGRAM

2.1 | Materials

This study utilized a normal concrete mix composed of ordinary Portland cement (OPC) with a specific gravity of 3.15, crushed stone as a coarse aggregate (maximum size 15 mm, specific gravity 2.67), and sand as a natural fine aggregate (fineness modulus of 2.51, specific gravity 2.62). In addition, two distinct sizes of CR aggregates: 5 mm (CR 5 mm) and No. 20 (CR No. 20) (which has a maximum nominal size of 0.825 mm), were used as a substitute for the natural fine aggregate, as shown in Figure 1. The specific gravity of CR 5 mm and CR No. 20 was 1.21 and 1.02, respectively.

A sieve analysis test was performed according to ASTM C136[43] to determine the particle size distribution of both the mineral aggregates and CR particles, as shown in Figure 2. Moreover, the grading limits specified in ASTM C33 for conventional aggregates and ASTM C330 for lightweight aggregates are also included for comparison purposes. As shown in Figure 2a,b, the grading curves of the natural aggregates generally follow the ASTM C33 grading envelopes and fall within or near the specified limits. Since CR (Figure 2c) is a recycled lightweight material rather than a conventional mineral aggregate, these specifications are used only as reference grading envelopes and are not intended as acceptance criteria for the CR particles employed in this study.

2.2 | Concrete mix

The concrete mixtures were proportioned in accordance with the ACI 211.1 standard method for selecting proportions for normal-weight concrete mixtures.[44] The incorporation of CR as a partial volumetric replacement of fine aggregate was subsequently implemented while maintaining the target water-to-cement ratio and workability requirements. Three groups of concrete mixes were prepared, as listed in Table 1. The first group

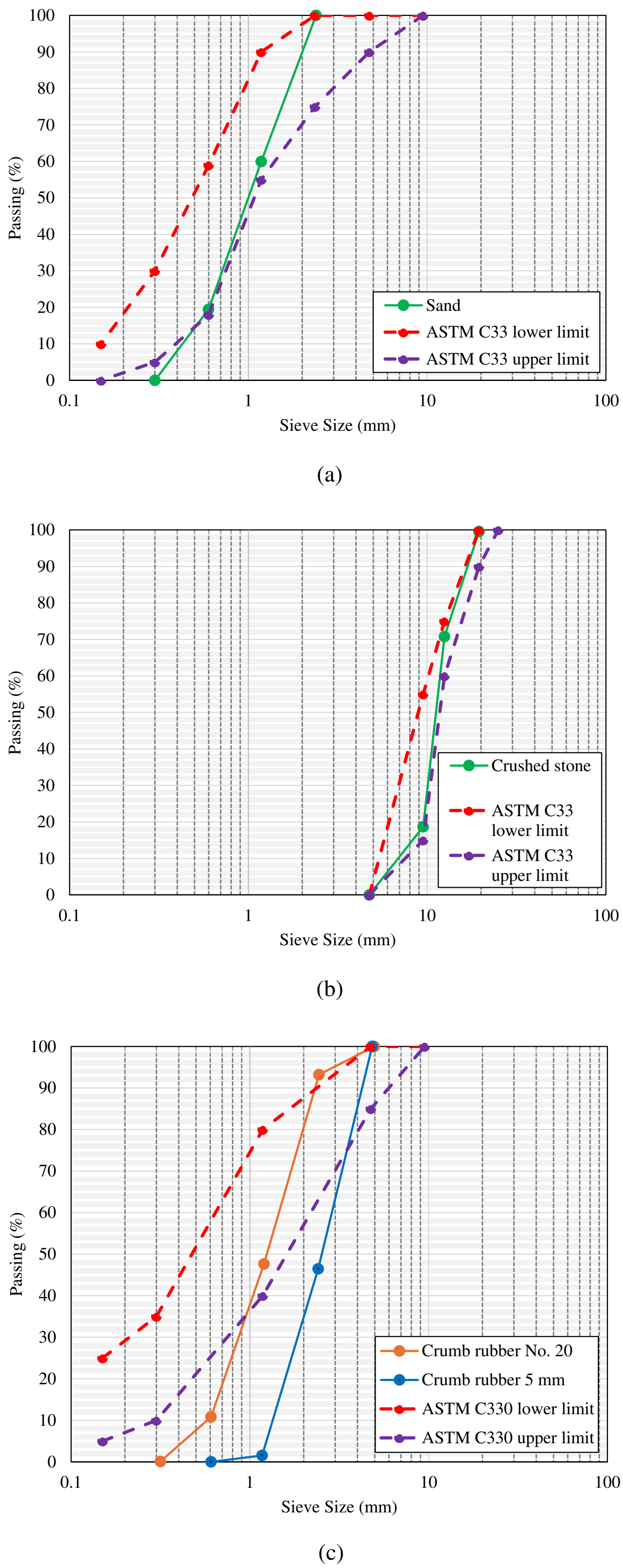

FIGURE 2 Practical size distribution curves of the used aggregates: (a) Natural fine aggregate (Sand); (b) Crushed stone aggregate; (c) Crumb rubber (CR) aggregate.

(Control) consisted of one mix with natural fine aggregate (sand). In the second (CR 5 mm) and third (CR No. 20) groups, the natural aggregate was replaced with a CR aggregate, either 5 mm or No. 20 particle size, respectively, as a partial replacement for fine aggregate at 5%, 10%, 15%, and 20% by volume. The concrete mixes were labeled as follows: the first letters specify the concrete type (natural concrete [N], CRC [C]), the next digit indicates the rubber particle size (no replacement [0], 5 mm [5], and No. 20 particle size [No. 20]), and the last number represents substitution level (0%, 5%, 10%, 15%, and 20%), as presented in Table 1. For example, the specimen N-0-0 refers to natural aggregate concrete without CR aggregate, and C-5-15 denotes CRC containing 5 mm rubber particles with 15% rubber content.

2.3 | Reinforcement

Deformed steel bars and BFRP bars were used in this study, as shown in Figure 3. The BFRP bars were manufactured via automated pultrusion using a composite mixture of 70% basalt fibers and 30% vinyl ester resin by volume. Two BFRP bar diameters, 12 and 16 mm, were considered for tensile reinforcement. However, 8- and 12-mm steel bar diameters were adopted for stirrups and tensile reinforcement, respectively. The axial tensile tests of the steel bars were conducted according to ASTM A370,[45] whereas the tensile properties of the BFRP bars were determined following ASTM D7205/D7205M,[46] and the average results were summarized in Table 2. The stress–strain relationships of the steel and BFRP reinforcement bars obtained from the axial tensile tests are presented in Figure 4.

2.4 | Tested beams

Fifteen reinforced concrete beams were designed and constructed with dimensions of 150 × 250 × 1850 mm, as shown in Figure 5. The steel-RC beams were designed with 2Φ12 steel bars (reinforcement configurations type 1) as an under-reinforced section ($\rho_s \leq \rho_{s,b}$) using Equations 1a and 1b to fail by steel yielding and then concrete crushing. However, two different reinforcement configurations were proposed for the BFRP-RC beams; type 1: 2Φ12 and type 2: 3Φ16 as an over-reinforced section ($\rho_f \geq \rho_{f,b}$) using Equations 2a and 2b, and would fail due to crushing of the concrete in the compression zone without BFRP rupture. The clear concrete cover was 30 mm with a clear spacing. Shear reinforcement

TABLE 1 Concrete mix proportions.

Group	Specimen	Cement (kg/m^3)	Fine aggregate (kg/m^3)			Coarse aggregate (kg/m^3)	Water (kg/m^3)
			Sand	Crumb rubber 5 mm	Crumb rubber No. 20		
Control	N-0-0	400	567	-	-	1261	168
CR 5 mm	C-5-05	400	547	29	-	1261	168
	C-5-10	400	491	55	-	1261	168
	C-5-15	400	440	78	-	1261	168
	C-5-20	400	395	99	-	1261	168
CR No. 20	C-No.20-05	400	536	-	28	1261	168
	C-No.20-10	400	473	-	53	1261	168
	C-No.20-15	400	417	-	74	1261	168
	C-No.20-20	400	369	-	92	1261	168

FIGURE 3 Reinforcement bars.

comprised 8 mm diameter steel stirrups spaced at 125 mm, supplemented by two 10 mm diameter steel bars in the compression zone for construction stability, as shown in Figure 5.

$$\rho_s = \frac{A_s}{bd} \tag{1a}$$

$$\rho_{s,b} = \alpha_1 \beta_1 \frac{f_c{}'}{f_y} \frac{\varepsilon_{cu}}{\varepsilon_{cu} + \varepsilon_y} \text{with steel bars} \tag{1b}$$

$$\rho_f = \frac{A_f}{bd} \tag{2a}$$

$$\rho_{f,b} = \alpha_1 \beta_1 \frac{f_c{}'}{f_{fu}} \frac{\varepsilon_{cu}}{\varepsilon_{cu} + \varepsilon_f} \text{with BFRP bars} \tag{2b}$$

$$\alpha_1 = 0.85 \, \text{ACI 440.1R} - 15 \tag{3a}$$

$$\beta_1 = 0.85 - \frac{0.05(f'_c - 27.6)}{6.9} \text{ACI 440.1R} - 15 \tag{3b}$$

$$\alpha_1 = 0.97 - 0.0025 f'_c \geq 0.67 \, \text{CSA S806} - 12 \tag{4a}$$

$$\beta_1 = 0.85 - 0.0015 f'_c \geq 0.67 \, \text{CSA S806} - 12 \tag{4b}$$

where ρ_s and ρ_f are the steel and BFRP reinforcement ratios, respectively, A_s and A_f are the areas of steel and BFRP bars, respectively (mm^2), b is the beam width (mm), d_s and d_f are the effective depths of steel and BFRP bars, respectively, (mm), α_1 is the ratio of the average stress of the equivalent rectangular stress block to the cylinder compressive strength of concrete, β_1 is the ratio of equivalent rectangular stress block to the depth of the neutral axis, $f_c{}'$ is the cylinder concrete compressive strength, f_y is the yield stress of the steel bars, ε_{cu} is the ultimate concrete strain in the compression zone, ε_y is the yield strain of the steel bars, and f_{fu} and ε_{fu} are the ultimate stress and strain of the BFRP bars, respectively.[36,37]

The experimental program consisted of three groups; the first group (Control) contains the beams cast with natural aggregate concrete served as a reference group; however, the second and third groups (CR 5 mm) and (CR No. 20) were CRC cast using CRC of 5 mm and No. 20 particle size, respectively, with different replacement ratios at 5%, 10%, 15%, and 20% by volume. The key parameters were concrete type, reinforcement type and ratio, rubber particle size, and replacement ratio. The tested beams were labeled as follows: the first letter specifies the concrete type (natural concrete [N], CRC [C]), the next letter indicates the reinforcement type (steel bars [S], BFRP bars [F]), the next number refers to the reinforcement configuration (type 1 [1], type 2 [2]), the following digit represents the rubber particle size (5 mm [5], No. 20 particle size [No. 20]), and the last number represents substitution level (5%, 10%, 15%, and

TABLE 2 Mechanical properties of reinforcement bars.

Bar type	D (mm)	Elastic modulus, E (GPa)	Yield strength, f_y (MPa)	Yield strain, ε_y (%)	Tensile strength, f_u (MPa)	Ultimate strain, ε_u (%)
BFRP	10	54	-	-	1322	2.46
	12	54	-	-	1301	2.43
	16	54	-	-	1267	2.35
Steel	8	200	481	0.24	604	5.24
	12	200	425	0.21	632	3.30

Abbreviation: BFRP, basalt fiber-reinforced polymer.

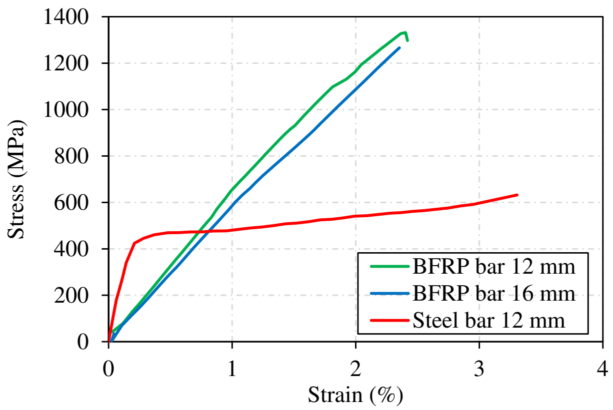

FIGURE 4 Stress–strain curves of basalt fiber-reinforced polymer (BFRP) and steel bars.

20%), as presented in Table 3. For instance, beam NS1-0-0 refers to a natural aggregate concrete beam without CR aggregate reinforced with 2Φ12 steel bars; however, CF2-5-15 denotes a CRC beam cast with 5 mm rubber particles with 15% rubber content and reinforced with 3Φ16 BFRP bars.

2.5 | Specimen preparation and casting procedure

All concrete mixtures were prepared using a rotary drum concrete mixer. Initially, the coarse aggregate, fine aggregate, and cement were dry-mixed to achieve a uniform distribution of the constituent materials. Subsequently, CR particles were gradually introduced as a partial volumetric replacement of fine aggregate, followed by the addition of water during continuous mixing to ensure adequate dispersion of the rubber particles within the concrete matrix. The mixing process was continued until a homogeneous mixture was obtained. Following mixing, the concrete was placed into the beam molds in successive layers and compacted using a mechanical vibrator to minimize entrapped air and ensure proper consolidation. The reinforcement cages and instrumentation locations were carefully fixed before casting to maintain the required concrete cover and reinforcement alignment. After casting, the specimens were covered with plastic sheets to minimize moisture loss and were demolded after 24 h. Subsequently, all specimens were cured under laboratory conditions in accordance with standard concrete curing practices until the testing age of 28 days.

2.6 | Test setup and instrumentation

The four-point bending tests were conducted on the beam specimens using a 2000 kN servo-hydraulic actuator with a stroke-controlled displacement rate of 0.6 mm/min, as illustrated in Figure 6. A steel spreader beam ensured uniform load distribution across the pure bending zone between loading points. During testing, the loading process was systematically paused at each 10 kN increment to allow precise measurement of maximum crack widths with a digital crack width tester. Deflection measurements were obtained through three Linear Variable Differential Transformers (LVDTs) positioned at mid-span and loading points. Reinforcement strain gauges were installed before casting, in addition to five concrete strain gauges that were arranged vertically along the mid-span cross-section. A computerized multi-channel data acquisition system was utilized for recording the measurements from the LVDTs and strain gauges. Additionally, crack width measurements were obtained using a handheld digital readout microscope with an accuracy of ±0.01 mm, allowing for meticulous tracking of crack propagation during loading pauses.

3 | TEST RESULTS AND DISCUSSION

3.1 | Fresh properties of the concrete mixes

Workability was assessed using the slump test in accordance with ASTM C143[47] and the results for the

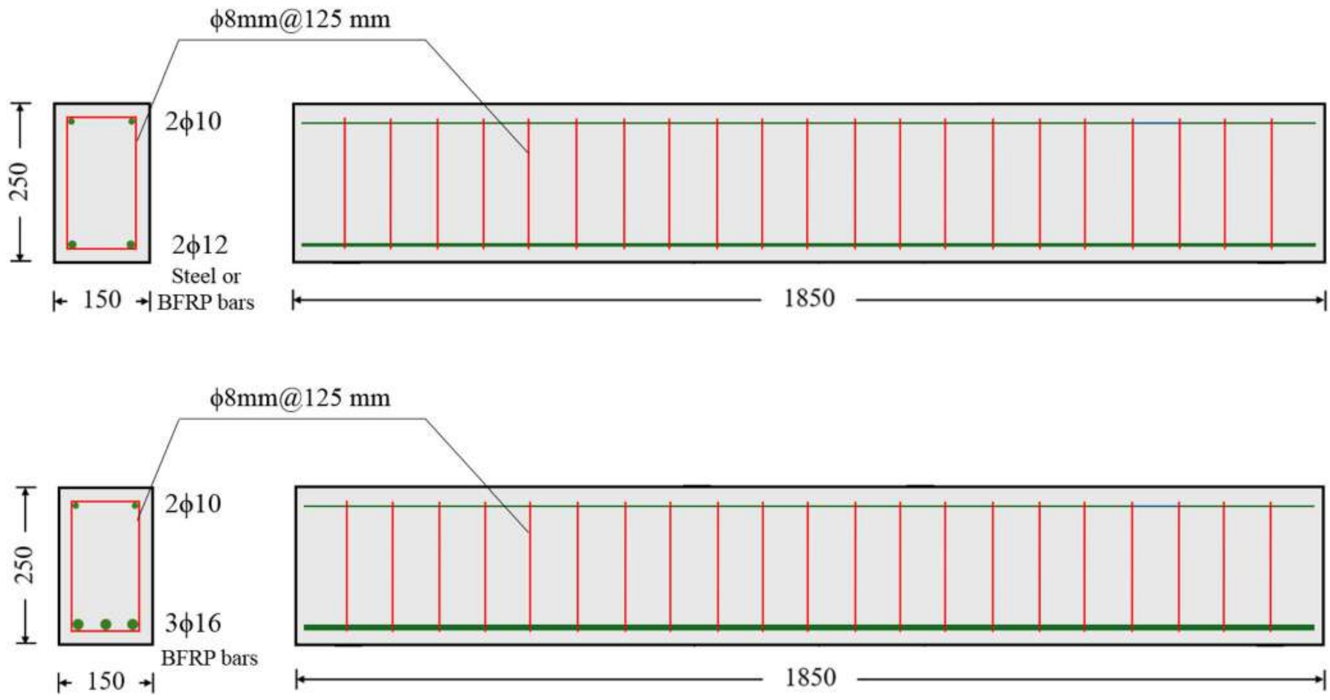

FIGURE 5 Geometrical details and reinforcement configurations of the tested beams (Dimensions in mm).

TABLE 3 Reinforcement details of the beam specimens.

Group	Beam	Reinforcement bars	Reinforcement ratio, ρ %	Balanced reinforcement ratio, $\rho_{s,b}$ or $\rho_{f,b}$ %	Section type
Control	NS1-0-0	2Φ12	0.73	3.67	Under-reinforced
	NF1-0-0	2Φ12	0.73	0.22	Over-reinforced
	NF2-0-0	3Φ16	1.97	0.24	Over-reinforced
CR 5 mm	CS1-5-05	2Φ12	0.73	3.67	Under-reinforced
	CF1-5-05	2Φ12	0.73	0.22	Over-reinforced
	CF2-5-05	3Φ16	1.97	0.24	Over-reinforced
	CF1-5-10	2Φ12	0.73	0.22	Over-reinforced
	CF1-5-15	2Φ12	0.73	0.22	Over-reinforced
	CF1-5-20	2Φ12	0.73	0.22	Over-reinforced
CR No. 20	CS1-No.20-05	2Φ12	0.73	3.67	Under-reinforced
	CF1-No.20-05	2Φ12	0.73	0.22	Over-reinforced
	CF2-No.20-05	3Φ16	1.97	0.24	Over-reinforced
	CF1-No.20-10	2Φ12	0.73	0.22	Over-reinforced
	CF1-No.20-15	2Φ12	0.73	0.22	Over-reinforced
	CF1-No.20-20	2Φ12	0.73	0.22	Over-reinforced

different concrete mixtures are summarized in Table 4. The target slump range for the designed concrete mix was selected between 30 and 50 mm. It was observed that the inclusion of CR consistently reduced the slump of CRC. In addition, a noticeable decrease in slump occurred as CR content increased, with a more pronounced reduction observed for the smaller rubber particles (No. 20), as illustrated in Figure 7. Specifically, raising the CR content from 5% to 20% resulted in slump reductions of approximately 4%–19% for 5 mm particles and 8%–25% for No. 20 particles. This reduction in slump can be attributed to several factors: (1) the irregular and non-uniform shapes of the rubber particles increase interparticle friction, thereby

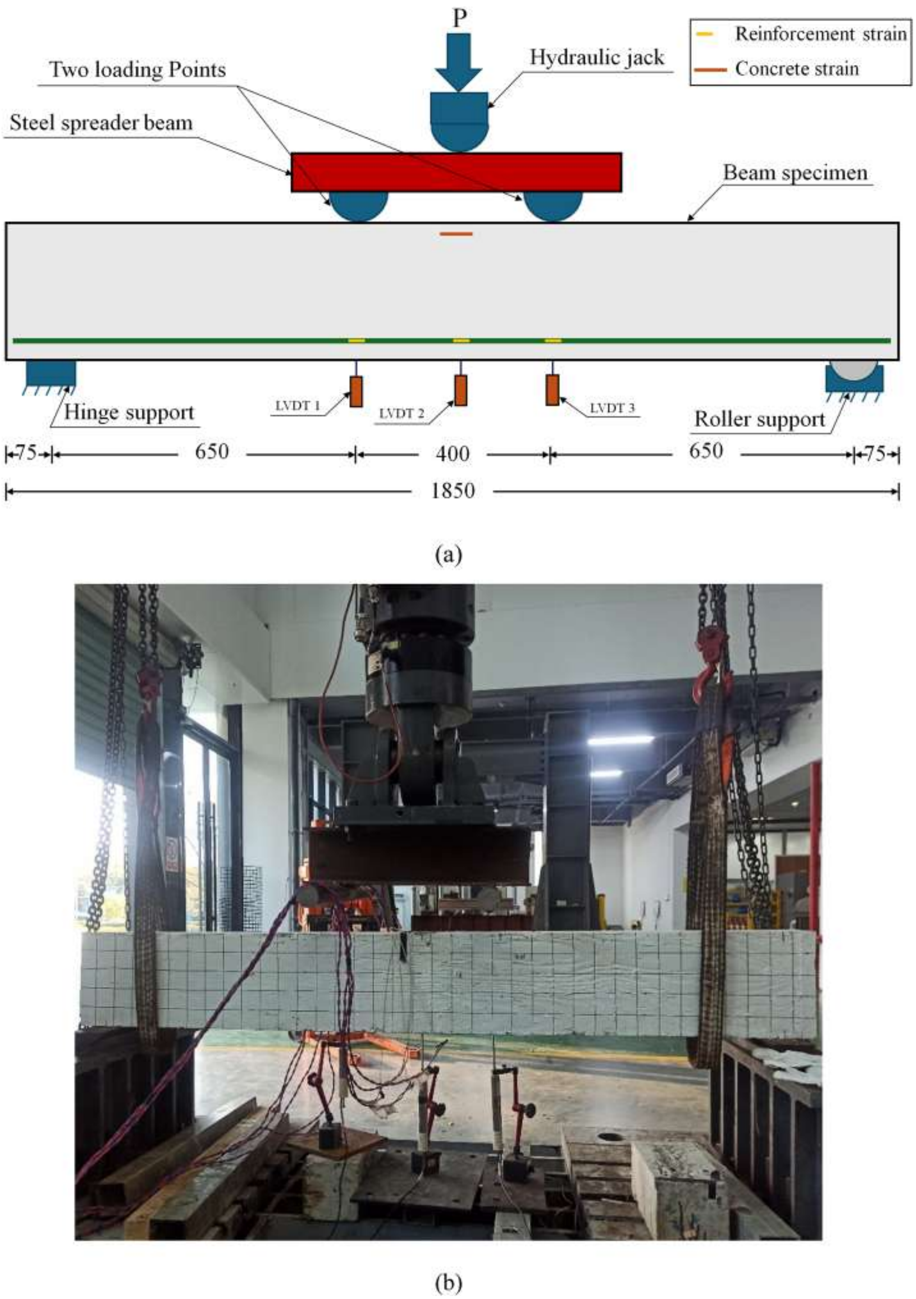

FIGURE 6 Overview of test setup: (a) Schematic drawing; (b) Beam specimen ready for testing (Dimensions in mm).

reducing flowability[3]; (2) the rougher surface texture of rubber particles, compared to sand, increases internal friction among the concrete constituents and raises resistance to flow.[48]

Fresh concrete density was determined in accordance with ASTM C138/C138M.[49] As illustrated in Table 4, replacing natural sand with CR significantly reduced the density of the concrete mixtures, with the reduction becoming more pronounced as the replacement ratio increased. This behavior is primarily attributed to the substantially lower specific gravity of CR compared with natural sand.[3] The specific gravities of the 5 mm and No. 20 CR particles were 1.21 and 1.02, respectively, whereas the corresponding value for natural sand was 2.62. Consequently, the 5 mm and No. 20 CR particles were approximately 54% and 61% lighter than sand, respectively. At identical replacement ratios, mixtures incorporating No. 20 CR consistently exhibited lower densities than those containing 5 mm particles due to the lower specific gravity of the finer rubber. For mixtures containing 5 mm CR, density reductions of approximately 7%, 11%, 15%, and 21% were observed at replacement levels of 5%, 10%, 15%, and 20%, respectively. Corresponding reductions for mixtures containing No. 20 CR were approximately 8%, 14%, 18%, and 24%.

TABLE 4 Fresh concrete properties.

Group	Specimen	Slump (mm)	Density (kg/m^3)
Control	N-0-0	48	2233
CR 5 mm	C-5-05	46	2079
	C-5-10	45	1982
	C-5-15	42	1894
	C-5-20	39	1775
CR No. 20	C-No.20-05	44	2052
	C-No.20-10	42	1916
	C-No.20-15	39	1821
	C-No.20-20	36	1703

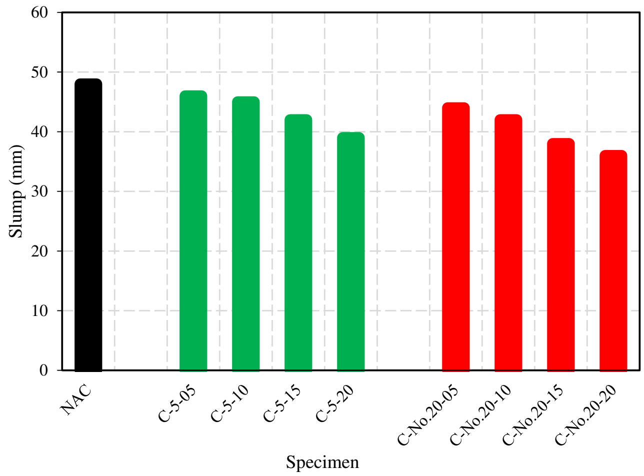

FIGURE 7 Slump results of the test specimens.

These results demonstrate the effectiveness of CR incorporation in producing lighter concrete mixtures and are consistent with previous studies reporting density reductions in rubberized concrete due to the low density and elastic nature of rubber particles.[16,50,51] Furthermore, the significant reduction in density highlights the potential of CR as a lightweight aggregate substitute. For this reason, the grading characteristics of the CR particles were also compared with the ASTM C330 grading envelopes for lightweight aggregates in Figure 2. Although CR is a recycled polymeric material and not a conventional lightweight mineral aggregate, the comparison provides useful insight into its particle-size distribution relative to materials commonly used in lightweight concrete applications. Overall, these results demonstrate the effectiveness of CR incorporation in producing lightweight cementitious composites. Furthermore, several mixtures satisfied the lightweight concrete classification requirements specified by ACI Committee 213,[52] highlighting the potential of CRC as a sustainable lightweight construction material.

3.2 | Hardened properties of the concrete mixes

3.2.1 | Compressive strength

Figure 8 illustrates the influence of CR aggregate on the hardened concrete properties. As shown in Figure 8a, the compressive strength of specimen C-5-05, containing 5% 5 mm CR, showed a 13% increase compared to natural concrete, as listed in Table 5. This may be attributed to improved particle packing and stress redistribution at low CR contents.[3] While all other mixes showed a reduction in compressive strength as the rubber content increased, regardless of the rubber particle size. The compressive strength decreased by 4%, 18%, and 25% for mixtures containing 10%, 15%, and 20% of 5 mm CR, respectively. Corresponding reductions of 9%, 25%, 34%, and 50% were observed for mixtures incorporating No. 20 CR at replacement levels of 5%, 10%, 15%, and 20%, respectively. This strength reduction primarily stems from increased porosity induced by rubber inclusion and increasing the replacement ratio led to interfacial debonding between CR particles and the cementitious matrix under compressive loading, and non-uniform distribution of rubber particles during casting, due to their lower specific gravity.[53,54] Moreover, rubber tends to migrate toward the top surface of molds during vibration, weakening the upper concrete layers.[55]

Moreover, Figure 8a demonstrates that finer CR particles (No. 20 sieve size) significantly reduce concrete compressive strength compared to natural concrete and CRC with 5 mm rubber particles, with strength losses escalating from 9% at 5% replacement to 50% at 20% replacement. This pronounced strength degradation is due to the inherently weaker interfacial bonding between the smooth, hydrophobic surfaces of fine rubber particles and cement paste compared to conventional sand-cement interfaces, and the greater elastic deformability of smaller rubber particles, which compromises stress transfer efficiency within the composite matrix.[3]

3.2.2 | Flexural strength

The flexural strength results are listed in Table 5 and presented in Figure 8b, exhibiting trends consistent with the compressive strength behavior, though with some notable distinctions. Concrete incorporating 5% of 5 mm CR showed a modest 5% increase in flexural strength, potentially due to improved energy absorption and microcrack arresting capabilities of the rubber particles.[3] However, higher replacement ratios of 10%, 15%, and 20% led to progressive strength reductions of 7%, 27%, and 38%,

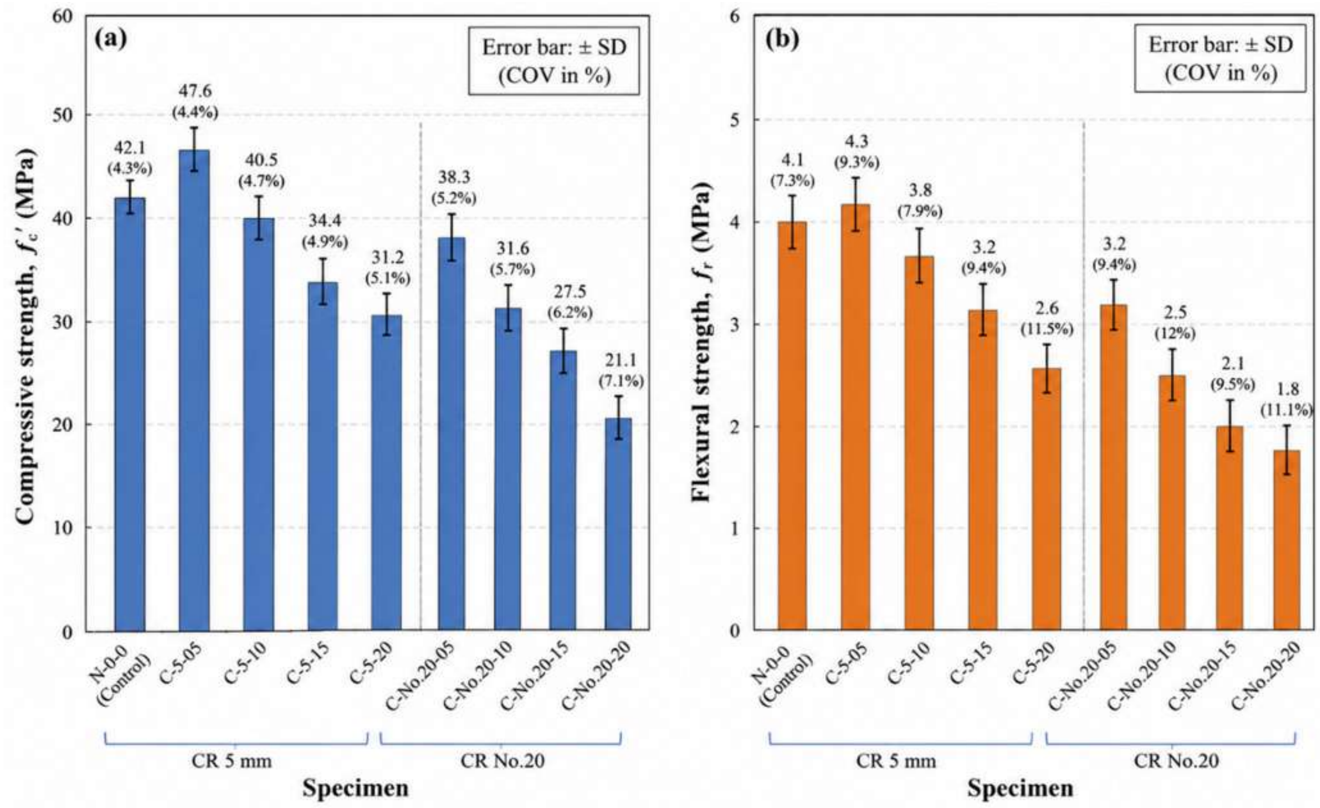

FIGURE 8 Hardened concrete properties of different concrete mixes: (a) Compressive strength, and (b) Flexural strength.

TABLE 5 Hardened concrete properties.

Group	Specimen	Compressive strength f_c' (MPa)	SD (MPa)	COV (%)	Flexural strength f_r (MPa)	SD (MPa)	COV (%)
Control	N-0-0	42.1	±1.8	4.3	4.1	±0.3	7.3
CR 5 mm	C-5-05	47.6	±2.1	4.4	4.3	±0.4	9.3
	C-5-10	40.5	±1.9	4.7	3.8	±0.3	7.9
	C-5-15	34.4	±1.7	4.9	3.2	±0.3	9.4
	C-5-20	31.2	±1.6	5.1	2.6	±0.3	11.5
CR No. 20	C-No.20-05	38.3	±2.0	5.2	3.2	±0.3	9.4
	C-No.20-10	31.6	±1.8	5.7	2.5	±0.3	12
	C-No.20-15	27.5	±1.7	6.2	2.1	±0.2	9.5
	C-No.20-20	21.1	±1.5	7.1	1.8	±0.2	11.1

Abbreviations: COV: coefficient of variation; SD: standard deviation.

respectively. This performance degradation primarily stems from two interrelated mechanisms: (1) the weakened rubber-cement matrix interface resulting from inadequate chemical bonding between hydrophobic rubber surfaces and cement paste,[56] and (2) reduced mechanical interlocking at higher rubber contents as reported in previous studies.[20,57] The effect was further exacerbated when using finer No. 20 CR particles, where the smoother surface texture and higher specific surface area decreased interfacial shear resistance, resulting in more pronounced flexural strength reductions of 22%–56% across the 5%–20% replacement range. These findings collectively demonstrate that while CR incorporation can marginally enhance the mechanical properties at low dosages, the trade-off between improved deformation capacity and strength reduction becomes increasingly unfavorable at higher replacement levels, particularly with finer rubber particles.[3]

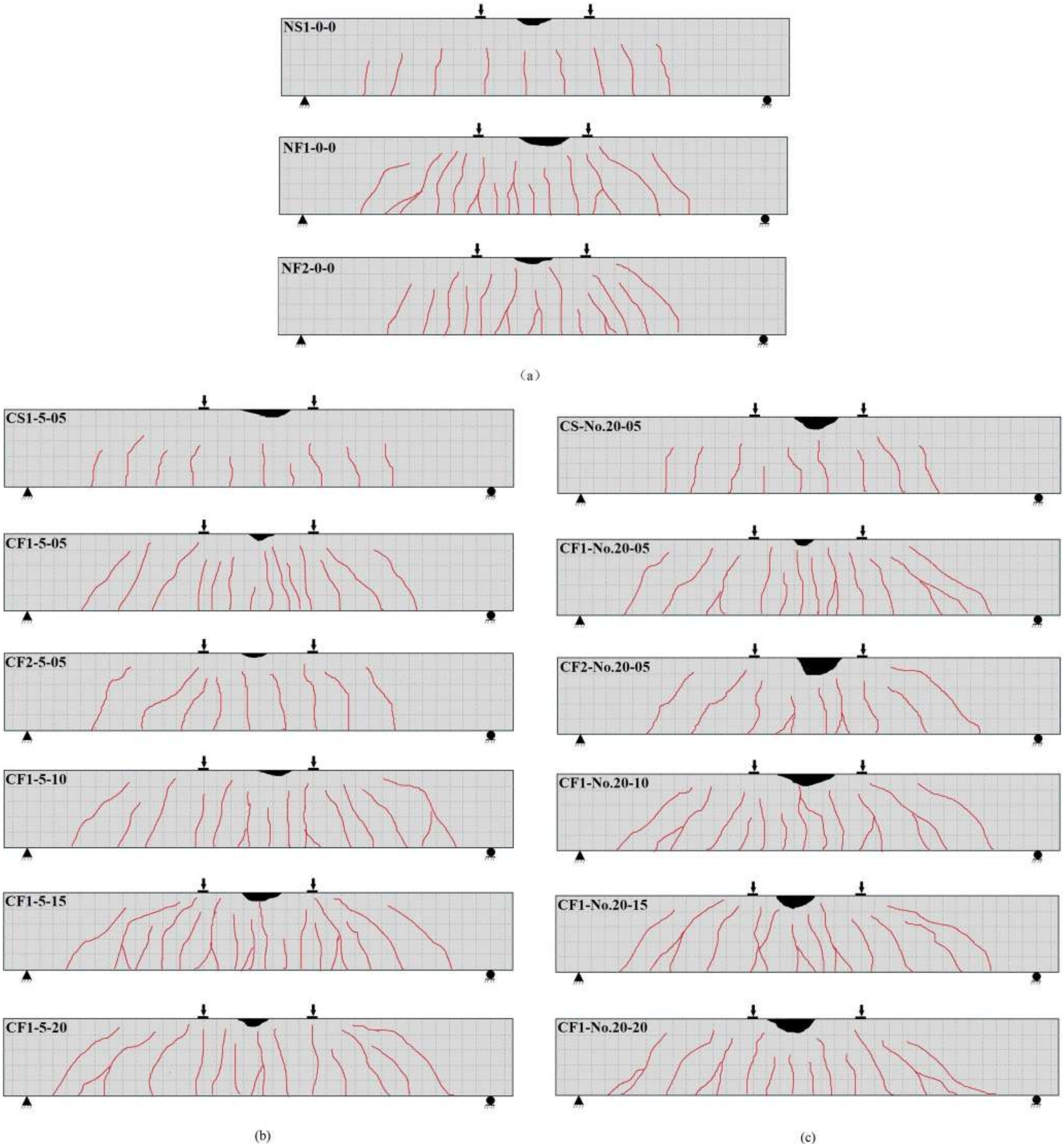

FIGURE 9 Cracking patterns and failure modes of all tested beams: (a) Control; (b) CR 5 mm; (c) CR No. 20.

3.3 | Cracking patterns and failure modes of the tested beams

Figure 9 illustrates the typical crack development pattern observed in all tested beams, demonstrating characteristic flexural cracking behavior consistent with conventional simply supported beam theory, regardless of the concrete type. Crack initiation occurred in the maximum moment region, manifesting as vertical cracks oriented perpendicular to the principal tensile stresses generated by pure bending action. As loading progressed, additional flexural cracks were formed in the constant moment zone, resulting in smaller crack spacing. Compared with steel-RC beams, the BFRP-RC beams exhibited wider crack spacing and larger crack widths at similar load levels due to the lower elastic modulus of BFRP bars.[58] This behavior reduced the crack control efficiency of the reinforcement and resulted in more pronounced crack propagation.[41] Nevertheless, the cracks in BFRP-RC beams remained more uniformly distributed over the pure bending zone, particularly in beams with higher reinforcement ratios. The increase in BFRP reinforcement ratio significantly influenced the cracking behavior and failure characteristics. Beams reinforced with 3Φ16 BFRP bars (NF2 and CF2 series) exhibited a larger number of finer cracks and delayed crack localization compared with beams reinforced with 2Φ12 bars. This behavior indicates improved stress distribution and higher flexural stiffness after cracking.[59]

Incorporation of CR noticeably altered the visual cracking characteristics of the concrete beams. Generally, CRC beams exhibited more distributed cracking patterns and larger deformation before failure compared with normal concrete beams. This behavior may be attributed to the higher deformability and energy absorption capacity of CR particles, which enhanced the post-cracking deformational response of the concrete matrix.[60] Increasing the CR replacement ratio resulted in earlier crack initiation, increased crack density, and more irregular crack trajectories. At higher replacement levels, several cracks propagated diagonally toward the supports, indicating reduced stiffness and lower tensile resistance of the CRC. Furthermore, beams incorporating finer CR particles (No. 20) showed more numerous and closely spaced cracks compared with beams containing 5 mm rubber particles. This phenomenon is associated with the larger surface area and weaker interfacial bonding of finer rubber particles with the cement matrix, which accelerates microcrack formation and propagation.[61]

Regardless of the concrete type, steel-RC beams exhibited a typical flexural failure mode by concrete crushing at the top face after yielding of steel bars, as shown in Figure 10a. This failure is also characterized by uniformly distributed vertical cracks initiating from the tension zone and propagating toward the loading region, indicating a stable and ductile cracking mechanism. However, BFRP-RC beams showed fewer but more pronounced inclined cracks extending toward the supports, reflecting a tendency toward brittle behavior and reduced crack redistribution capacity compared to steel-RC beams. Collapsed in flexural mode, precipitated by concrete crushing in the compression zone without tensile rupture of the BFRP bars, as shown in Figure 10b.

3.4 | Cracking load

The cracking load for each beam is listed in Table 6. The test results indicate a clear influence of reinforcement type, reinforcement ratio, and rubber characteristics. Steel-reinforced beams exhibited slightly higher cracking loads compared to their BFRP counterparts, as seen in NS1-0-0 (23.4 kN·m) versus NF1-0-0 (22.6 kN·m), due to the higher stiffness of steel which delays crack initiation. Increasing the BFRP reinforcement ratio had a marginal effect on cracking load, with NF2-0-0 (24.1 kN·m) only slightly exceeding NF1-0-0, confirming that cracking is primarily governed by concrete tensile strength rather than reinforcement amount. In contrast, rubber content had a pronounced negative effect, where increasing rubber from 5% to 20% reduced the cracking load significantly (e.g., CF1-5-05: 23.2 kN·m to CF1-5-20: 14.8 kN·m), attributed to the weakening of the concrete matrix. Similarly, using finer rubber particles (No. 20) further reduced cracking load compared to 5 mm rubber (e.g., CS1-5-05: 23.8 kN·m vs. CS1-No.20-05: 16.6 kN·m), indicating reduced tensile strength with finer rubber dispersion.

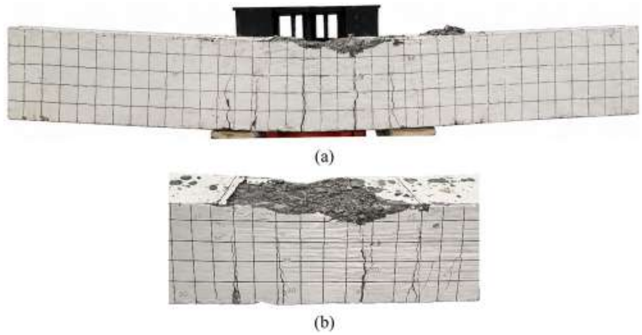

FIGURE 10 Typical flexural failure of the tested beams: (a) CS1-5-05; (b) CF1-5-10.

3.5 | Ultimate load

Regardless of the concrete type, the influence of reinforcement type becomes dominant where the BFRP-RC beams showed significantly higher ultimate loads than their counterparts, steel-RC beams, as seen in NF1-0-0 (108 kN·m) compared to NS1-0-0 (67 kN·m), due to the higher tensile strength of BFRP bars. Table 6 demonstrated that increasing the BFRP reinforcement ratio led to a substantial increase of 34.3% in ultimate load from 108 kN·m in beam NF1-0-0 to 145 kN·m in beam NF2-0-0, highlighting the strong contribution of reinforcement capacity at failure. However, the incorporation of CR led to a decrease in the ultimate load, and this reduction becomes significant with increasing the rubber content from CF1-5-05: 113 to CF1-5-20: 79 kN, for 5 mm rubber particles, reflecting the reduction in compressive strength and stiffness of CRC. Moreover, the effect of

TABLE 6 Test results of the beams.

Beam	Cracking load, P_{cr} (kN)	Cracking deflection, Δ_{cr} (mm)	Yielding load, P_y (kN)	Yielding deflection, Δ_y (mm)	Ultimate load, P_u (kN)	Ultimate deflection, Δ_u (mm)
NS1-0-0	23.4	1.7	48.8	7.3	67.6	45.1
NF1-0-0	22.6	2.1	-	-	108.1	42.9
NF2-0-0	24.1	1.3	-	-	141.2	39.5
CS1-5-05	23.8	0.9	51.1	6.8	70.6	46.2
CF1-5-05	23.2	1.1	-	-	113.7	41.3
CF2-5-05	24.6	0.8	-	-	146.3	44.1
CF1-5-10	21.4	2.2	-	-	97.5	43.7
CF1-5-15	18.2	2.4	-	-	88.2	39.8
CF1-5-20	14.8	2.8	-	-	81.4	39.1
CS1-No.20-05	16.6	1.2	51	9.4	62.9	31.3
CF1-No.20-05	15.3	1.5	-	-	98.4	45.2
CF2-No.20-05	19.2	1.1	-	-	130.3	58.4
CF1-No.20-10	15.8	2.5	-	-	93.4	46.6
CF1-No.20-15	12.4	2.6	-	-	83.7	49.2
CF1-No.20-20	10.2	2.9	-	-	71.1	46.1

rubber size also appears significant, where beams with finer rubber (No. 20) generally exhibited lower ultimate loads compared to those with 5 mm rubber at the same content. For example, CF1-5-05 reached 113 kN; however, CF1-No.20-05 yielded 98 kN. Overall, while cracking load is mainly governed by concrete properties and is adversely affected by rubber inclusion, ultimate load is strongly controlled by reinforcement type and ratio, with BFRP and higher reinforcement ratios enhancing capacity, while higher rubber content and finer particles reduce it.

3.6 | Load-deflection relationship

Figure 11 presents the load-deflection behavior of the tested beams. The load–deflection curves provide a clear picture of how reinforcement type, reinforcement ratio, rubber content, and rubber particle size affected the full flexural response of the beams from loading initiation up to failure. In general, all specimens exhibited an initial nearly linear response before cracking, followed by a reduction in stiffness after cracking, and then a progressive approach to peak load. However, the shape of the curves and the extent of stiffness degradation varied markedly with the studied parameters. The stiffness of CRC was found to be less than natural concrete due to the soft texture and lower elastic modulus of CR compared to natural aggregate.[16,50] Figure 11a shows that beam NS1-0-0 showed the classical response of an under-reinforced member, with a relatively steep initial slope, a distinct change in slope after cracking, and then a yielding stage followed by large deflection growth with only limited load increase, which confirms a ductile flexural behavior. By contrast, the BFRP-RC beams NF1-0-0 and NF2-0-0 did not exhibit a yielding plateau because BFRP bars remain linearly elastic up to failure. Their curves continued rising after cracking with no sudden flattening, and their peak loads were much higher than that of the steel beam. This reflects the high tensile strength of BFRP reinforcement, although the absence of yielding indicates a less ductile failure mechanism compared with steel reinforcement.

The effect of reinforcement type is especially evident when comparing NS1-0-0 with NF1-0-0, and CS1-5-05 with CF1-5-05. The steel-RC beams exhibited greater stiffness in the early loading stage and a more recognizable elastic–cracked–yielding sequence, whereas the BFRP-RC beams showed a smoother transition from the uncracked to cracked stage and maintained load growth over a wider range after cracking. This behavior can be attributed to the fundamental difference between steel and BFRP bars: steel has a lower tensile strength but yields and redistributes stresses, while BFRP has high tensile strength but no yielding stage. Consequently, the BFRP-RC beams developed substantially larger ultimate loads, while the steel-RC beams showed clearer ductility and warning before failure. This distinction remained valid in both natural concrete and CRC beams.

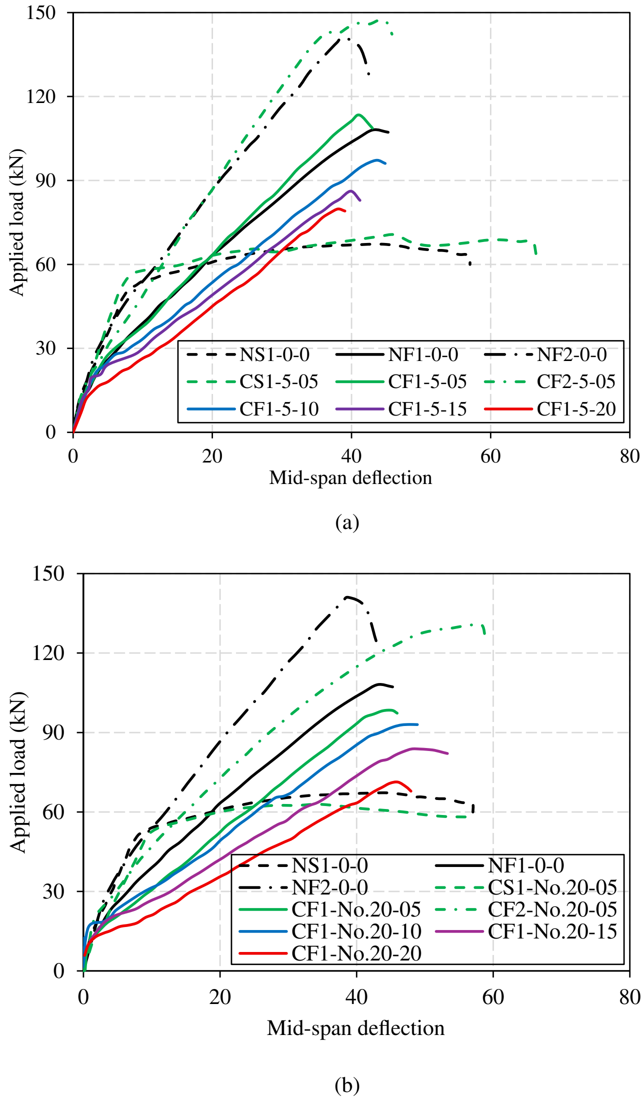

FIGURE 11 Load-mid-span deflection relationships of the tested beams: (a) Control and CR 5 mm groups, and (b) Control and CR No. 20 groups.

The reinforcement ratio had a very pronounced influence on the curve shape, stiffness after cracking, and ultimate resistance. This is clear from the comparison between NF1-0-0 and NF2-0-0 in natural concrete, as well as between CF1-5-05 and CF2-5-05 or CF1-No.20-05 and CF2-No.20-05 in CRC, as shown in Figure 10b. Increasing the BFRP reinforcement ratio shifted the entire curve upward, increased the post-cracking slope, and led to significantly higher peak load. In addition, beams with a higher reinforcement ratio generally exhibited lower deflection at a given load level, which indicates better resistance to flexural deformation. The higher amount of longitudinal reinforcement increased the flexural rigidity after cracking and delayed the development of large tensile strains in the bars, thereby improving the load-carrying capacity. At the same time, the high-ratio beams tended to fail in a more sudden manner once the compression zone was exhausted, which is consistent with their over-reinforced classification shown in the experimental program.

The influence of rubber content is very clear in both groups of CRC beams. Regarding rubber content, the results show that beams incorporating 5% CR with 5 mm particle size (e.g., CF1-5-05 and CF2-5-05) exhibited relatively improved performance compared to higher rubber contents, with lower deflection, higher stiffness, and greater ultimate load. However, as the rubber content increased from 10% to 20%, the curves progressively shifted downward and became flatter, indicating a reduction in stiffness and load-carrying capacity due to the smooth rubber surface texture that reduces interfacial shear resistance.[23] This suggests that a low rubber content (around 5%) may provide a balanced performance, while higher contents significantly degrade structural behavior.[42] The effect of rubber particle size is also evident, where beams with 5 mm rubber generally showed better stiffness and higher ultimate loads compared to those with finer rubber (No. 20), as shown in Figure 11b. Overall, the beams containing finer rubber particles (No. 20) tended to show lower cracking resistance and lower ultimate load than the beams containing 5 mm rubber. This suggests that the finer rubber particles caused a greater reduction in concrete compactness and matrix continuity and the poor interfacial bonding between finer rubber particles and the cement paste.[62] This phenomena resulted in lower stiffness, hence larger deflection ranges, which may indicate improved deformability, but this came with a clear reduction in load capacity.

3.7 | Load-crack width relationship

Figure 12 shows the load–crack width curves for the tested beams. It can be seen that there is a clear influence of reinforcement type, reinforcement ratio, rubber content, and rubber particle size on crack development and propagation throughout the loading stages. In terms of reinforcement type, steel-RC beams (NS and CS series) exhibited narrower crack widths compared to BFRP-RC beams due to the high elastic modulus of steel bars. However, a rapid increase in the crack width after yielding, where relatively small increases in load resulted in significant crack widening, reflects the yielding behavior of steel and stress redistribution along the cracks. On the other hand, BFRP-RC beams (NF and CF series) showed a more gradual and continuous increase in crack width with load, without a yielding point, indicating a more stable but less ductile crack propagation governed by the

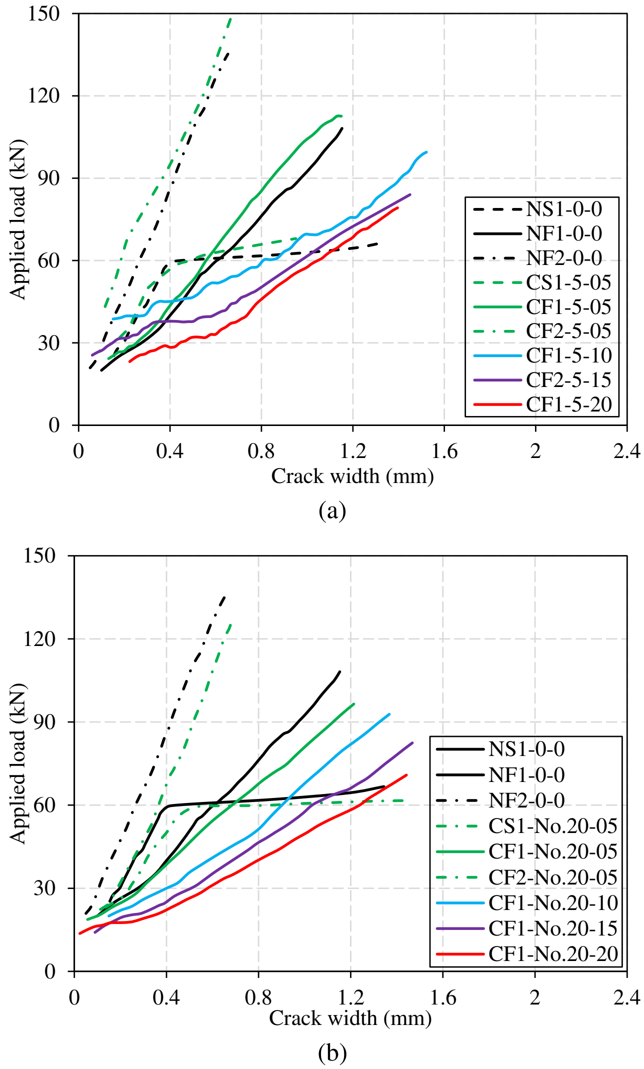

FIGURE 12 Load-Crack width relationships of the tested beams: (a) Control and CR 5 mm groups, and (b) Control and CR No. 20 groups.

linear-elastic behavior of BFRP bars compared to steel-RC beams. At comparable load levels, NF1-0-0 and CF1-05-5 beams generally exhibited larger crack widths than CS1-0-0 and CS1-05-5 beams, respectively (see Figure 12a), which can be attributed to the lower modulus of elasticity of BFRP, resulting in reduced crack control.

Increasing the BFRP reinforcement ratio (compared to NF1 and CF1) significantly improved crack control. Beams NF2-0-0 and CF2-5-05 resulted in smaller crack widths at the same load levels and steeper load–crack width curves than NF1-0-0 and CF1-5-05, indicating that additional reinforcement enhances the distribution of tensile stresses and limits crack opening. A similar trend was observed when comparing beam CF1-5-05 with beam CF2-5-05 and beam CF1-No.20–05 with beam CF2-No.20–05, as shown in Figure 12b, where the higher ratio beams sustained higher loads at lower crack widths. Regarding rubber content, the curves show that beams with 5% CR (e.g., CF1-5-05 and CF2-5-05) exhibited better crack control, with smaller crack widths at comparable load levels than NF1-0-0 and NF2-0-0. As the rubber content increased from 10% to 20%, the curves progressively shifted toward larger crack widths for a given load, indicating reduced crack resistance due to the weakness of the concrete matrix. However, finer CR particle sizes (No. 20) lead to a wider crack width through all replacement ratios compared to the natural concrete, as shown in Figure 12b. Thus, higher rubber content led to earlier crack opening and faster crack propagation, which is consistent with the reduced tensile strength and stiffness of CRC.

By comparing the beams in CR 5 mm and CR No. 20 groups incorporating 5 mm rubber generally exhibited better crack control, maintaining smaller crack widths at higher load levels compared to beams with finer rubber (No. 20). The No. 20 specimens showed wider cracks at similar loads, indicating that finer rubber particles resulted in weaker matrix integrity and reduced ability to restrain crack growth.

3.8 | Load-strain relationship

The load–reinforcement strain curves for the tested beams are shown in Figure 13. Regarding concrete type, natural concrete beams (NS and NF series) exhibited higher load levels at lower reinforcement strains compared to CRC beams, indicating better stiffness and more efficient stress transfer to the reinforcement, while CRC beams showed a more gradual increase in load with significantly higher strains, reflecting their reduced stiffness and increased deformability. In terms of reinforcement type, steel-RC beams (NS and CS series) displayed a distinct yielding region characterized by a plateau in load despite increasing strain, confirming ductile behavior and stress redistribution after yielding. In contrast, BFRP-RC beams (NF and CF series) exhibited a continuous linear increase in load with strain up to failure, without any yielding plateau, resulting in higher ultimate strains due to the lower modulus of elasticity of BFRP bars but a more brittle failure mode. The reinforcement ratio had a significant effect, whereas increasing the BFRP ratio (NF2-0-0 and CF2-5-05 compared to NF1-0-0 and CF1-5-05) led to higher load capacity at lower strain levels, indicating improved stiffness and more efficient load transfer, as well as a reduction in strain at comparable load levels. Regarding rubber content, beams with 5% rubber (e.g., CF1-5-05 and CF2-5-05) exhibited relatively better performance with higher loads and lower strains

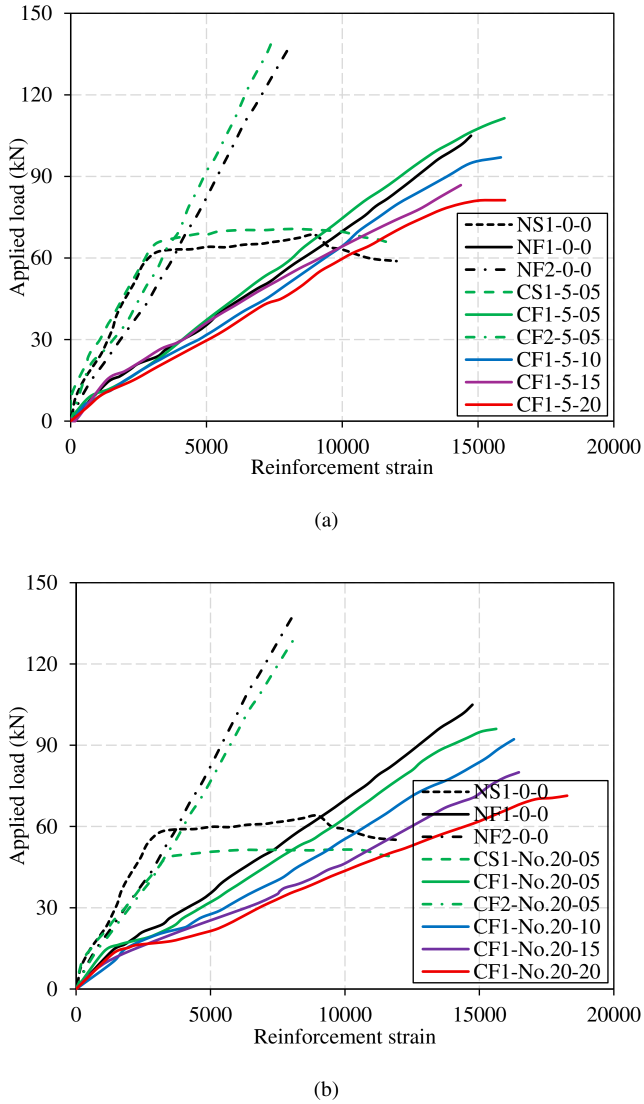

FIGURE 13 Load-reinforcement strain relationships of the tested beams: (a) Control and CR 5 mm groups, and (b) Control and CR No. 20 groups.

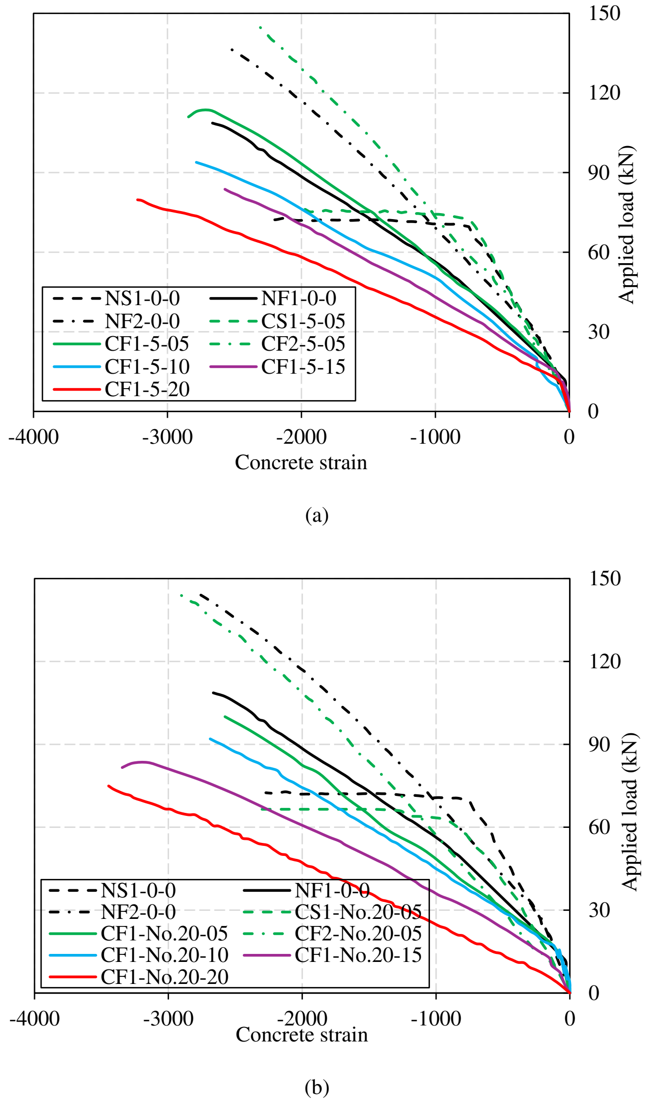

FIGURE 14 Load-concrete strain relationships of the tested beams: (a) Control and CR 5 mm groups, and (b) Control and CR No. 20 groups.

compared to beams with higher rubber contents, as shown in Figure 13a.

As the rubber content increased from 10% to 20%, the curves displayed higher strain values at lower loads, demonstrating reduced stiffness and strength due to the weakening of the concrete matrix. Moreover, the effect of rubber particle size is evident when comparing CR 5 mm and CR No. 20 series, where beams with 5 mm rubber generally showed higher load levels and lower corresponding strains than those with finer rubber (No. 20) (see Figure 13b), suggesting that larger rubber particles resulted in less severe degradation of mechanical properties. However, replacing the natural aggregate with CR No. 20 led to higher BFRP strain records and this effect becomes more pronounced as the substitution ratio of CR increases.

Figure 14 shows the load–concrete strain curves of the tested beams. Incorporating crumb rubber, changing the reinforcement type, increasing the reinforcement ratio, and varying the rubber content and particle size all had a marked influence on the compressive response of the beams. Compared with the natural concrete beams, the CRC beams generally exhibited a more gradual increase in compressive strain with load, indicating lower stiffness of the compression zone and a softer overall response, as shown in Figure 14a. Additionally, increasing the BFRP reinforcement ratio, as seen in beams NF2-0-0 and CF2-5-05 compared with NF1-0-0 and CF1-5-05, resulted in higher load capacity accompanied by larger compressive strains in the concrete, indicating that the concrete compression zone became more heavily mobilized as the tensile resistance of the reinforcement increased. At 5% rubber replacement, the beams still maintained relatively high load levels with substantial concrete strain development, especially in CF1-5-05 and CF2-5-05, whereas increasing the rubber content from 10% to 20% progressively reduced the slope of the curves and lowered the corresponding load carried at a given concrete strain, confirming that higher rubber content weakened the concrete matrix and reduced the efficiency of stress transfer in compression.

The effect of rubber particle size can be observed by comparing the CR 5 mm and CR No. 20 groups. At the same load level, the beams containing 5 mm rubber generally developed lower compressive strains than the corresponding beams with No. 20 rubber (Figure 14b), indicating better performance of the coarser rubber particles. Overall, the curves confirm that CR incorporation reduced the stiffness and compressive resistance of the beams, but this adverse effect was less pronounced at low rubber content and with larger particle size.

The experimental results obtained in this study are generally consistent with previous investigations on CRC and FRP-reinforced concrete members. Similar to the findings reported by Son et al.[32] and Al-Tayeb et al.[33] increasing the CR replacement ratio resulted in reductions in compressive strength, flexural strength, cracking resistance, and load-carrying capacity. These reductions have been widely attributed to the weak interfacial bond between rubber particles and the cementitious matrix as well as the increased deformability of rubber inclusions. The present study further demonstrated that the reduction in structural performance becomes more pronounced when finer CR particles are used, highlighting the importance of particle size in structural applications. The observed increase in deformability and more distributed cracking patterns of CRC beams also agree with previous studies that reported enhanced energy absorption capacity and ductility in rubberized concrete members. Furthermore, the behavior of BFRP-reinforced beams was consistent with the findings reported for FRP-reinforced concrete structures, where higher ultimate load capacities were achieved at the expense of reduced ductility due to the linear-elastic behavior of FRP reinforcement. The results additionally showed that increasing the BFRP reinforcement ratio effectively improved post-cracking stiffness and ultimate flexural capacity.

4 | THEORETICAL BACKGROUND AND ANALYTICAL FORMULATIONS

4.1 | Prediction of cracking load

The cracking moment, M_{cr} is the moment based on the first visible crack and it can be determined through the expression given in Equation (5) and the cracking load, $P_{cr,pre}$ is calculated as presented in Equation (6) follows:

$$M_{cr} = \frac{f_r I_g}{y_t} \quad (5)$$

$$P_{cr,pre} = 2 M_{cr} / 0.65 \quad (6)$$

where I_g is the gross moment of inertia, y_t is the vertical distance between the extreme tension fibers and the neutral axis, and f_r is the flexural strength of the concrete.

Table 7 presents the cracking prediction with the design previsions. The predictions for the cracking load of the tested beams showed an average $P_{cr}/P_{cr,pre.}$ of 1.17 ± 0.07, indicating that the predictive model tends to slightly underestimate the cracking load. This trend is consistent across the control, CR 5 mm, and CR No. 20 groups, suggesting that the adopted formulation is conservative in predicting the onset of cracking for CRC-RC beams. The variability becomes more noticeable in beams with higher rubber content or different reinforcement configurations, particularly in the CR No. 20 group. This indicates a stronger influence of larger rubber particle sizes and modified stiffness characteristics on delaying crack initiation compared to predictions.

TABLE 7 Comparison between the experimental and predicted Cracking load.

Group	Beam	P_{cr}	$\frac{P_{cr}}{P_{cr,pre.}}$
Control	NS1-0-0	23.4	1.17
	NF1-0-0	22.6	1.13
	NF2-0-0	24.1	1.21
CR 5 mm	CS1-5-05	23.8	1.15
	CF1-5-05	23.2	1.12
	CF2-5-05	24.6	1.19
	CF1-5-10	21.4	1.16
	CF1-5-15	18.2	1.18
	CF1-5-20	14.8	1.19
CR No. 20	CS1-No.20-05	16.6	1.09
	CF1-No.20-05	15.3	1.00
	CF2-No.20-05	19.2	1.26
	CF1-No.20-10	15.8	1.32
	CF1-No.20-15	12.4	1.21
	CF1-No.20-20	10.2	1.17
Average			1.17
Standard deviation			0.07
Coefficient of variation (%)			6.2

4.2 | Prediction of ultimate load

To evaluate the applicability of existing design provisions for predicting the flexural capacity of CRC beams reinforced with BFRP bars, the experimental ultimate loads were compared with the predictions obtained from several international design codes and analytical approaches. The predicted flexural capacity of FRP-RC beams for ACI 440.1R-15,[36] CSA S806-12,[37] AASHTO LRFD, the Chinese FRP design recommendations Gb 50608-2020,[63] JSCE provisions,[64] SP295,[65] and Eurocode 2 (EC2)[66] is presented in Table 8.

The comparison was conducted using the ratio between the experimental and predicted ultimate loads $P_{\mathrm{u,exp.}}/P_{\mathrm{u,pre.}}$, where values greater than unity indicate conservative predictions, as listed in Table 9. The comparison results demonstrated that most of the considered design approaches provided reasonably conservative predictions for the flexural capacity of the tested beams. Among the evaluated models, the ACI 440.1R and AASHTO LRFD provisions showed identical prediction trends, resulting in an average $P_{\mathrm{ul,exp.}}/P_{\mathrm{ul,pre.}}$ ratio of approximately 1.10, indicating slightly conservative estimations of the ultimate capacity. Similarly, the CSA S806 and JSCE approaches also provided satisfactory agreement with the experimental results, with average ratios of 1.08 and 1.09, respectively. These results confirm the suitability of strain compatibility approaches combined with equivalent rectangular stress block assumptions for predicting the flexural behavior of BFRP-CRC beams.

The Chinese design approach and the Eurocode 2 (EC2) showed the closest agreement with the experimental results, with average $P_{\mathrm{ul,exp.}}/P_{\mathrm{ul,pre.}}$ ratios close to unity (approximately 1.01). This indicates excellent prediction accuracy and demonstrates that these models can effectively capture the flexural response of CRC beams reinforced with BFRP bars when the actual material properties are considered in the analysis. In contrast, the SP295 model generally produced unconservative predictions, resulting in an average ratio of approximately 0.93, indicating a tendency to overestimate the flexural capacity of the tested beams. The prediction trends also revealed that the agreement between analytical and experimental results remained satisfactory despite the reduction in concrete strength caused by increasing CR content. This observation suggests that the current FRP flexural design formulations remain applicable for CRC beams provided that the reduced mechanical properties of CRC are properly incorporated into the calculations. Furthermore, the prediction accuracy was generally maintained for both rubber particle sizes (5 mm and No. 20), although slightly larger deviations were observed for mixtures containing finer rubber particles due to their more pronounced influence on stiffness degradation and crack propagation behavior.

TABLE 8 Flexural Capacity Equations for FRP-RC Beams.

References	Equation
ACI 440.1R-15[36]	$M_u=\rho_f f_f\left(1-0.59\frac{\rho_f f_f}{f_c{}'}\right)bd^2$ $f_f=\sqrt{\frac{(E_f\varepsilon_{cu})^2}{4}+E_f\varepsilon_{cu}\left(\frac{0.85\beta_1 f_c{}'}{\rho_f}\right)}-\frac{(E_f\varepsilon_{cu})}{2}\leq f_{fu}$
CSA S806-12[37]	$M_u=\alpha_1\beta_1 f'_c cb\left(d-\frac{\beta_1 c}{2}\right)$ $c=\left(\frac{\rho_f f_f}{\alpha_1\,\beta_1 f'_c}\right)d$ $f_f=\sqrt{\frac{(E_f\varepsilon_{cu})^2}{4}+E_f\varepsilon_{cu}\left(\frac{\alpha_1\beta_1 f_c{}'}{\rho_f}\right)}-\frac{(E_f\varepsilon_{cu})}{2}\leq f_{fu}$
AASHTO LRFD[67]	$M_n=A_f\times f_f\times(d-a/2)$ $a=(A_f\times f_f)/(0.85\times f_c{}'\times b)$ $f_f=E_f\times\varepsilon_f$ $\varepsilon_f=\varepsilon_{cu}\times((d-c)/c)$ $c=a/\beta_1$
Gb 50608-2020[63]	$M_u=A_f\times f_f\times(h_0-x/2)$ $x=(A_f\times f_f)/(\alpha_1\times f_c\times b)$ $f_f=E_f\times\varepsilon_f$ $\varepsilon_f=\varepsilon_{cu}\times((h0-x)/x)$
JSCE	$M_u=T\times z$ $T=A_f\times f_f$ $z=d-(k_2\times x/2)$ $x=(A_f\times f_f)/(k_1\times k_3\times f_c{}'\times b)$
SP295[65]	$Mu=R_f\times f_f\times z$ $z=d-0.5x$ $x=(R_f\times f_f)/(R_b\times b)$
Eurocode 2[66]	$Mu=A_f\times f_f\times(d-\lambda x/2)$ $x=(A_f\times f_f)/(\eta\times f_{cd}\times b)$ $f_f=E_f\times\varepsilon_f$ $\lambda=0.8\,and\,\eta=1.0$
ACI 318[68]	$M_u=A_s f_y\left(d-\frac{\beta_1 c}{2}\right)$

4.3 | Practical implications for structural design

The findings of this study have important practical implications for the development of sustainable and durable concrete infrastructure. The incorporation of CR as a partial replacement of fine aggregate provides an environmentally responsible solution for recycling waste tires while simultaneously reducing the self-weight of concrete members. Furthermore, the use of BFRP reinforcement eliminates corrosion-related deterioration, making such structural systems particularly attractive for marine structures, bridge decks, parking structures, coastal facilities, and other aggressive environments where steel corrosion represents a major durability concern. Although the

TABLE 9 Comparison between the experimental and predicted Ultimate load results.

Beam	$P_{ul,exp.}$	$\left(\frac{P_{ul,exp.}}{P_{ul,pre.}}\right)_{ACI}$	$\left(\frac{P_{ul,exp.}}{P_{ul,pre.}}\right)_{CSA}$	$\left(\frac{P_{ul,exp.}}{P_{ul,pre.}}\right)_{AAASHTO}$	$\left(\frac{P_{ul,exp.}}{P_{ul,pre.}}\right)_{Chinese}$	$\left(\frac{P_{ul,exp.}}{P_{ul,pre.}}\right)_{JSCE}$	$\left(\frac{P_{ul,exp.}}{P_{ul,pre.}}\right)_{SP295}$	$\left(\frac{P_{ul,exp.}}{P_{ul,pre.}}\right)_{EC2}$
NS1-0-0	67.6	1.16	1.16	1.16	1.16	1.16	1.16	1.16
NF1-0-0	108.1	1.18	1.16	1.17	1.03	1.13	0.92	1.03
NF2-0-0	141.2	1.06	1.03	1.06	0.92	1.02	0.83	0.92
CS1-5-05	70.6	1.21	1.21	1.20	1.20	1.20	1.20	1.20
CF1-5-05	113.7	1.18	1.18	1.18	1.01	1.11	0.90	1.01
CF2-5-05	146.3	1.05	1.03	1.04	0.89	0.98	0.79	0.89
CF1-5-10	97.5	1.08	1.07	1.07	0.95	1.04	0.85	0.95
CF1-5-15	88.2	1.04	1.04	1.04	0.95	1.04	0.84	0.95
CF1-5-20	81.4	1.00	1.00	1.00	0.92	1.02	0.83	0.92
CS1-No.20-05	62.9	1.08	1.08	1.08	1.08	1.08	1.08	1.08
CF1-No.20-05	98.4	1.11	1.11	1.11	0.99	1.09	0.88	0.99
CF2-No.20-05	130.3	1.02	1.00	1.02	0.90	1.00	0.81	0.90
CF1-No.20-10	93.4	1.15	1.14	1.14	1.05	1.16	0.94	1.05
CF1-No.20-15	83.7	1.10	1.09	1.10	1.02	1.13	0.92	1.02
CF1-No.20-20	71.1	1.07	1.06	1.09	1.02	1.13	0.91	1.02
Average		1.10	1.08	1.10	1.00	1.09	0.93	1.00
Standard deviation		0.06	0.06	0.06	0.09	0.07	0.13	0.09
Coefficient of variation (%)		5.62	5.84	5.62	9.10	6.09	13.66	9.10

incorporation of CR reduced strength and stiffness, the tested beams maintained satisfactory structural performance and predictable flexural behavior. The experimental results demonstrated that the adverse effects of CR can be partially compensated through appropriate selection of reinforcement ratio and rubber particle size. The analytical comparisons confirmed that existing international FRP design provisions can reasonably predict the flexural capacity of BFRP-reinforced CRC beams, facilitating their implementation in practical structural design. Therefore, BFRP-reinforced CRC members represent a promising structural solution that combines environmental sustainability, enhanced durability, reduced maintenance requirements, and acceptable structural performance, thereby advancing resilient and sustainable construction practices.

5 | CONCLUSIONS

This study experimentally investigated the flexural behavior of concrete beams incorporating CR as a partial replacement of fine aggregate and reinforced with BFRP bars. A total of 15 beams were tested under four-point bending to evaluate the influence of key parameters, including concrete type (natural and CR concrete), reinforcement type (steel and BFRP bars) and ratio, CR content (5% to 20%, step 5%), and particle size (5 mm and No. 20). The structural performance was assessed in terms of cracking behavior, failure modes, load-carrying capacity, load–deflection response, crack width development, and strain characteristics. The experimental results were further compared with existing design provisions to examine their applicability for CRC beams reinforced with BFRP bars. The conclusions can be drawn as follows:

1. A low replacement ratio (5% with 5 mm particles) enhanced compressive strength by 13% and flexural strength by 5%, whereas higher replacement levels (10%–20%) progressively reduced strength, stiffness, cracking load, and ultimate capacity due to increased porosity and weaker rubber–cement bonding. For structural applications, a rubber replacement ratio of 5%–10% with 5 mm particles is recommended.
2. Beams containing 5 mm CR particles consistently exhibited higher load-carrying capacity, greater stiffness, and better crack control than those incorporating finer No. 20 particles, which resulted in more pronounced strength degradation and wider crack widths.
3. Steel-reinforced beams exhibited higher cracking loads and a ductile failure mode characterized by steel yielding prior to failure, whereas BFRP-reinforced beams achieved 60%–110% higher ultimate load capacities but

exhibited linear-elastic behavior up to failure with wider crack widths and reduced ductility.

4. Increasing the BFRP reinforcement ratio from 0.73% to 1.97% significantly improved cracking resistance, post-cracking stiffness, crack control, and ultimate flexural capacity by approximately 30%. However, higher reinforcement ratios promoted a more compression-controlled failure mode.
5. CRC beams exhibited greater deformability and more distributed cracking patterns than conventional concrete beams, demonstrating enhanced energy absorption capacity. However, this improvement was accompanied by reductions in stiffness and load-carrying capacity, highlighting the trade-off between ductility enhancement and strength reduction.
6. The predictions obtained from ACI 440.1R, CSA S806, AASHTO LRFD, JSCE, SP295, and Eurocode-based approaches showed reasonable agreement with the experimental results, confirming the applicability of existing FRP design provisions for BFRP-reinforced CRC beams.

The results demonstrate that BFRP-reinforced CRC beams can provide a sustainable and durable structural solution by combining waste tire recycling with corrosion-resistant reinforcement. These findings contribute to the growing body of knowledge on environmentally friendly concrete structures and support their potential application in bridge decks, parking structures, and marine infrastructure. Furthermore, the authors are currently conducting an ongoing research project to investigate additional aspects of BFRP-reinforced CRC systems, including long-term durability, fatigue performance, serviceability behavior, and life-cycle sustainability to facilitate their broader implementation in structural engineering practice.

ACKNOWLEDGMENTS

The International Science & Technology Cooperation Program of China (no. 2024YFE0198400), the National Natural Science Foundation of China (No. 52278244), and the Fundamental Research Funds for the Central Universities (No. 2242024k30039, 2242024k30050).

CONFLICT OF INTEREST STATEMENT

The authors declare no conflicts of interest.

DATA AVAILABILITY STATEMENT

Data will be made available on request.

ORCID

Yahia M. S. Ali https://orcid.org/0000-0002-8378-9275
Xin Wang https://orcid.org/0000-0003-4504-8502

NOMENCLATURE

A_f	Area of FRP reinforcement
A_s	Area of steel reinforcement
b	Beam width
c	distance from extreme fiber in compression to neutral axis
d	Effective depth from compression face to centroid of tension reinforcement
E_f	Elastic modulus of FRP bars
f_{cd}	Design value of concrete compressive strength
f_c'	Concrete compressive strength
f_f	Stress in FRP bars
f_r	Modulus of rupture (flexural tensile strength) of concrete
f_{fu}	Ultimate tensile strength of BFRP bars
h	Total depth of beam section
h_0	Effective depth used in Chinese provisions
I_g	Gross moment of inertia of the concrete section
k_1	JSCE stress block coefficient
k_2	JSCE lever arm coefficient
k_3	JSCE concrete stress coefficient
M_{cr}	Cracking moment
M_u	Ultimate moment
P_{cr}	Applied load at cracking
$P_{cr,pre}$	predicted load at cracking
P_u	Applied load at ultimate
$P_{u,pre}$	Applied load at ultimate
P_y	Applied load at yielding
R_b	Design compressive resistance of concrete (SP295)
R_f	Design tensile resistance of FRP reinforcement (SP295)
x	Neutral axis depth
y_t	Distance from neutral axis to extreme tension fiber
z	Internal lever arm
α_1	ratio of average concrete stress to concrete strength
β_1	ratio of depth of equivalent rectangular stress block to depth of neutral axis
Δ_{cr}	deflection at cracking
Δ_y	deflection at yielding
Δ_u	deflection at ultimate
ε_{cu}	Ultimate concrete strain
ε_f	FRP strain
ε_{fu}	Ultimate tensile strain of BFRP bars
ε_y	yielding strain of steel bars
η	Eurocode concrete stress block factor
λ	Eurocode stress block depth factor
ρ_f	reinforcement ratio of longitudinal FRP bars
$\rho_{f,b}$	balanced reinforcement ratio for FRP-RC members in which concrete crushing and FRP rupture occur synchronously

ρ_s reinforcement ratio of longitudinal steel bars
$\rho_{s,b}$ balanced reinforcement ratio in which concrete crushing and the yielding of steel bars occur synchronously

ORCID

Yahia M. S. Ali https://orcid.org/0000-0002-8378-9275
Xin Wang https://orcid.org/0000-0003-4504-8502

REFERENCES

1. Zhang Z, Ma H, Qian S. Investigation on properties of ECC incorporating crumb rubber of different sizes. J Adv Concrete Technol. 2015;13:241–51. https://doi.org/10.3151/jact.13.241
2. Mohammed BS, Loong RCH. Structural behavior of reinforced Rubbercrete beams in shear. Appl Mech Mater. 2015;752–753: 513–7. https://doi.org/10.4028/www.scientific.net/amm.752-753.513
3. Ali YMS, Wang X, Wu Z. Mechanical performance enhancement of crumb rubber concrete with basalt minibars. Arch Civ Mech Eng. 2026;26:1–21. https://doi.org/10.1007/s43452-026-01548-9
4. Abdo A, Sharaky IA, Eisa A, Ahmed S. Flexural behavior of steel/GFRP reinforced concrete beams having layered sections integrated with normal and rubberized concrete. Structure. 2024;70:107633. https://doi.org/10.1016/j.istruc.2024.107633
5. Ahmed S, Elshazli MT, Zaghlal M, Alashker Y, Abdo A. Improving shear behavior of rubberized concrete beams through sustainable integration of waste tire steel fibers and treated rubber. J Build Eng. 2024;96:110649. https://doi.org/10.1016/j.jobe.2024.110649
6. Nematzadeh M, Hosseini SA, Ozbakkaloglu T. The combined effect of crumb rubber aggregates and steel fibers on shear behavior of GFRP bar-reinforced high-strength concrete beams. J Build Eng. 2021;44:102981. https://doi.org/10.1016/j.jobe.2021.102981
7. Ahmed S, Sharaky IA, El Sayed S, Hassan H, Abdo A. Effect of rubberized concrete integrating uncoated and coated crumb rubber on the flexural behavior of the RC beams reinforced with steel and GFRP bars. Construct Build Mater. 2024;426:136192. https://doi.org/10.1016/j.conbuildmat.2024.136192
8. Kaushik A, Prakash G, Rajput A. Influence of crumb rubber on the response of concrete beams against low velocity impact. Construct Build Mater. 2022;347:128614. https://doi.org/10.1016/j.conbuildmat.2022.128614
9. Aiello MA, Leuzzi F. Waste tyre rubberized concrete: properties at fresh and hardened state. Waste Manag. 2010;30:1696–704. https://doi.org/10.1016/j.wasman.2010.02.005
10. Pacheco-Torgal F, Ding Y, Jalali S. Properties and durability of concrete containing polymeric wastes (tyre rubber and polyethylene terephthalate bottles): an overview. Construct Build Mater. 2012;30:714–24. https://doi.org/10.1016/j.conbuildmat.2011.11.047
11. Tamanna K, Tiznobaik M, Banthia N, Shahria Alam M. Mechanical properties of rubberized concrete containing recycled concrete aggregate. ACI Mater J. 2020;117:169–80. https://doi.org/10.14359/51722409
12. Carroll JC, Helminger N. Fresh and hardened properties of fiber-reinforced rubber concrete. J Mater Civ Eng. 2016;28:1–9. https://doi.org/10.1061/(asce)mt.1943-5533.0001541
13. Onuaguluchi O, Panesar DK. Hardened properties of concrete mixtures containing pre-coated crumb rubber and silica fume. J Clean Prod. 2014;82:125–31. https://doi.org/10.1016/j.jclepro.2014.06.068
14. Youssf O, Mills JE, Hassanli R. Assessment of the mechanical performance of crumb rubber concrete. Construct Build Mater. 2016;125:175–83. https://doi.org/10.1016/j.conbuildmat.2016.08.040
15. Liu F, Zheng W, Li L, Feng W, Ning G. Mechanical and fatigue performance of rubber concrete. Construct Build Mater. 2013; 47:711–9. https://doi.org/10.1016/j.conbuildmat.2013.05.055
16. Su H, Yang J, Ling TC, Ghataora GS, Dirar S. Properties of concrete prepared with waste tyre rubber particles of uniform and varying sizes. J Clean Prod. 2015;91:288–96. https://doi.org/10.1016/j.jclepro.2014.12.022
17. Ismail MK, Hassan AAA. Ductility and cracking behavior of reinforced self-consolidating rubberized concrete beams. J Mater Civ Eng. 2017;29:1–10. https://doi.org/10.1061/(asce)mt.1943-5533.0001699
18. Xue J, Shinozuka M. Rubberized concrete: a green structural material with enhanced energy-dissipation capability. Construct Build Mater. 2013;42:196–204. https://doi.org/10.1016/j.conbuildmat.2013.01.005
19. Zheng L, Sharon Huo X, Yuan Y. Experimental investigation on dynamic properties of rubberized concrete. Construct Build Mater. 2008;22:939–47. https://doi.org/10.1016/j.conbuildmat.2007.03.005
20. Gupta T, Chaudhary S, Sharma RK. Assessment of mechanical and durability properties of concrete containing waste rubber tire as fine aggregate. Constr Build Mater. 2014;73:562–74. https://doi.org/10.1016/j.conbuildmat.2014.09.102
21. Guo H, Zhu H. Study on the structural properties of steel reinforced crc beam-cracking resistance. Adv Mater Res. 2012;374–377:775–80. https://doi.org/10.4028/www.scientific.net/AMR.374-377.775
22. Liu F, Chen G, Li L, Guo Y. Study of impact performance of rubber reinforced concrete. Construct Build Mater. 2012;36: 604–16. https://doi.org/10.1016/j.conbuildmat.2012.06.014
23. Li L, Ruan S, Zeng L. Mechanical properties and constitutive equations of concrete containing a low volume of tire rubber particles. Constr Build Mater. 2014;70:291–308. https://doi.org/10.1016/j.conbuildmat.2014.07.105
24. Thomas BS, Gupta RC, Kalla P, Cseteneyi L. Strength, abrasion and permeation characteristics of cement concrete containing discarded rubber fine aggregates. Constr Build Mater. 2014;59: 204–12. https://doi.org/10.1016/j.conbuildmat.2014.01.074
25. Sasania F, Nematzadeh M, Asadi M, Aminian A. Thermomechanical behavior of high-strength concrete with nylon granule aggregates: experimental evaluation and predictive analysis. Civ Eng Appl Solut. 2025;1:1–35. https://doi.org/10.22080/ceas.2025.29200.1011.Sasania
26. Ghatte HF, Nazari A. Prediction of Rice husk ash-based SCC compressive strength: data-driven framework. Civ Eng Appl Solut. 2025;1:17–28. https://doi.org/10.22080/ceas.2025.29625.1025.Farrokh

27. Sabeti N. Evaluation of setting behavior in slag-based Geopolymer concrete using ultrasonic pulse velocity under varying mix proportions. Civ Eng Appl Solut. 2025;1:48–61. https://doi.org/10.22080/ceas.2025.29600.1023.Sabeti
28. Nemati M, Aminian A, Rahimi S, Nematzadeh M, Jafarzadeh-Taleshi M, Thai HT. Compressive behavior of prestressed SFRCFST stub columns after heating: effect of fresh concrete compression technique. Case Stud Constr Mater. 2025;23:e04968. https://doi.org/10.1016/j.cscm.2025.e04968
29. Sabetifar H, Mousavimehr M, Aminian A, Nematzadeh M. Residual axial performance of PET/rubber-modified concrete confined with CFRP strips after thermal exposure: experimental and theoretical analysis. Dev Built Environ. 2026;25:100834. https://doi.org/10.1016/j.dibe.2025.100834
30. Hassanli R, Youssf O, Mills JE. Experimental investigations of reinforced rubberized concrete structural members. J Build Eng. 2017;10:149–65. https://doi.org/10.1016/j.jobe.2017.03.006
31. Mendis ASM, Al-Deen S, Ashraf M. Flexural shear behaviour of reinforced crumbed rubber concrete beam. Constr Build Mater. 2018;166:779–91. https://doi.org/10.1016/j.conbuildmat.2018.01.150
32. Son KS, Hajirasouliha I, Pilakoutas K. Strength and deformability of waste tyre rubber-filled reinforced concrete columns. Constr Build Mater. 2011;25:218–26. https://doi.org/10.1016/j.conbuildmat.2010.06.035
33. Al-Tayeb MM, Abu Bakar BH, Ismail H, Md Akil H. Effect of partial replacement of sand by fine crumb rubber on impact load behavior of concrete beam: experiment and nonlinear dynamic analysis. Mater Struct. 2013;46:1299–307. https://doi.org/10.1617/s11527-012-9974-3
34. Wu Z, Wang X. State-of-the-art of advanced FRP applications in civil infrastructure in Japan. Compos Polycon 2007. Tampa, FL USA: American Composites Manufacturers Association; 2007.
35. Elgabbas F, Vincent P, Ahmed EA, Benmokrane B. Experimental testing of basalt-fiber-reinforced polymer bars in concrete beams. Compos Part B Eng. 2016;91:205–18. https://doi.org/10.1016/j.compositesb.2016.01.045
36. ACI Committee 440. Guide for the design and construction of Structural Concrete Reinforced with Fiber-Reinforced Polymer (FRP) Bars (ACI 440.1R-15). ACI 440.1R-15. Farmington Hills, MI: American Concrete Institute; 2015.
37. CSA (Canadian Standards Association). Design and construction of building components with fibre reinforced polymers. CAN/CSA S806-12. Mississauga, ON, Canada: CSA; 2012.
38. Wu Z, Wang X, Wu G. Advancement of structural safety and sustainability with basalt fiber reinforced polymers. Proceedings of the 6th International Conference on FRP Composites in Civil Engineering; Ontario, Canada: International Institute for FRP in Construction (IIFC); 2012. p. 13–5.
39. Inman M, Rafn E, Azrague K. A mechanical and environmental assessment and comparison of basalt fibre reinforced polymer (BFRP) rebar and steel rebar in concrete beams. Energy Procedia. 2017;111:31–40. https://doi.org/10.1016/j.egypro.2017.03.005
40. Wang X, Wu Z, Wu G, Zhu H, Zen F. Enhancement of basalt FRP by hybridization for long-span cable-stayed bridge. Compos Part B. 2013;44:184–92. https://doi.org/10.1016/j.compositesb.2012.06.001
41. Elgabbas F, Ahmed EA, Benmokrane B. Flexural behavior of concrete beams reinforced with ribbed basalt-FRP bars under static loads. J Compos Constr. 2017;21:21. https://doi.org/10.1061/(ASCE)CC.1943-5614.0000752
42. Ali YMS, Wang X, Wu Z. Bond-slip behavior and failure mechanism of basalt-FRP bars with different surface treatments in crumb rubber concrete. Constr Build Mater. 2025;490:142464. https://doi.org/10.1016/j.conbuildmat.2025.142464
43. ASTM C136. Standard test method for sieve analysis of fine and coarse aggregates. ASTM Int 2012.
44. ACI-PRC-211. Selecting Proportions for Normal-Density and High-Density Concrete—Guide (ACI PRC-211.1-22). Farmington Hills: American Concrete Institute; 2022.
45. ASTM C33. Standard specification for concrete aggregates. 1999.
46. ASTM D7205/D7205M. Standard test method for tensile properties of fiber reinforced polymer matrix composite bars. 2016.
47. ASTM C143. Standard test method for slump of hydraulic-cement cosncrete. ASTM Int 2015.
48. B.S 1881. Testing concrete—Part 116: Method for determination of compressive strength of concrete cubes. 1983.
49. ASTM C138/C138M—13a. Standard test method for density (unit weight), yield, and air content (gravimetric); 2013. https://doi.org/10.1520/C0138
50. Gupta T, Chaudhary S, Sharma RK. Mechanical and durability properties of waste rubber fiber concrete with and without silica fume. J Clean Prod. 2016;112:702–11. https://doi.org/10.1016/j.jclepro.2015.07.081
51. Bisht K, Ramana PV. Evaluation of mechanical and durability properties of crumb rubber concrete. Constr Build Mater. 2017;155:811–7. https://doi.org/10.1016/j.conbuildmat.2017.08.131
52. ACI Committee (2014). ACI PRC-213-14: Guide for structural lightweight aggregate concrete. Farmington Hills: American Concrete Institute; 2023.
53. Topçu IB, Bilir T. Analysis of rubberized concrete as a three-phase composite material. J Compos Mater. 2009;43:1251–63. https://doi.org/10.1177/0021998308104226
54. Bignozzi MC, Sandrolini F. Tyre rubber waste recycling in self-compacting concrete. Cem Concr Res. 2006;36:735–9. https://doi.org/10.1016/j.cemconres.2005.12.011
55. Eisa AS, Elshazli MT, Nawar MT. Experimental investigation on the effect of using crumb rubber and steel fibers on the structural behavior of reinforced concrete beams. Constr Build Mater. 2020;252:119078. https://doi.org/10.1016/j.conbuildmat.2020.119078
56. Taha MMR, El-Dieb AS, El-Wahab MAA, Abdel-Hameed ME. Mechanical, fracture, and microstructural investigations of rubber concrete. J Mater Civ Eng. 2008;20:640–9. https://doi.org/10.1061/(ASCE)0899-1561(2008)20
57. Ganjian E, Khorami M, Maghsoudi AA. Scrap-tyre-rubber replacement for aggregate and filler in concrete. Constr Build Mater. 2009;23:1828–36. https://doi.org/10.1016/j.conbuildmat.2008.09.020
58. Jiang K, Wang X, Cheng C, Ding J, Liu S, Ali YMS. Durability assessment of BFRP-reinforced composite beams incorporating UHP-SSC permanent formwork under marine exposure. Eng Struct. 2026;363:123028. https://doi.org/10.1016/j.engstruct.2026.123028
59. Mendis ASM, Al-Deen S, Ashraf M. Effect of rubber particles on the flexural behaviour of reinforced crumbed rubber concrete beams. Constr Build Mater. 2017;154:644–57. https://doi.org/10.1016/j.conbuildmat.2017.07.220
60. Ismail MK, Hassan AAA. Performance of full-scale self-consolidating rubberized concrete beams in flexure. ACI Mater J. 2016;113:207–18. https://doi.org/10.14359/51688640

61. Hall MR, Najim KB. Structural behaviour and durability of steel-reinforced structural plain/self-compacting rubberised concrete (PRC/SCRC). Constr Build Mater. 2014;73:490–7. https://doi.org/10.1016/j.conbuildmat.2014.09.063
62. Najim KB, Hall MR. A review of the fresh/hardened properties and applications for plain- (PRC) and self-compacting rubberised concrete (SCRC). Constr Build Mater. 2010;24:2043–51. https://doi.org/10.1016/j.conbuildmat.2010.04.056
63. GB50608-2010. Technical Code for Infrastructure Application of FRP Composites. Beijing: China planning press; 2020.
64. JSCE (Japanese Society of Civil Engineering). Recommendation for design and construction of concrete structures using continuous fibre reinforcing materials. Tokyo: JSCE; 1997.
65. SP 295.1325800, Russian State Standard. Konstrukcii betonnye, armir- ovannye polimernoj kompozitnoj armaturoj. Pravila proektirovaniya. Obshchiye Tekhnicheskiye Usloviya [Concrete structures reinforced with fibre-reinforced polymer bars. Design rules]. 2017.
66. 2: E 1992-1-1. Eurocode 2: Design of concrete structures – Part 1–1: General rules and rules for buildings. EN 1992-1-1. Brussels, Belgium: European Committee for Standardization; 2004.
67. AASHTO LFRD. Bridge design guide specifications for GFRP–reinforced concrete. 2018.
68. ACI 318–19. Building code (ACI 318–19) and commentary on building code requirements for structural concrete (ACI 318R-19). 2019.

AUTHOR BIOGRAPHIES

Yahia M. S. Ali, Key Laboratory of C & PC Structures Ministry of Education, Southeast University, Nanjing 210096, China. Email: yahiaali@seu.edu.cn.

Xin Wang, Key Laboratory of C & PC Structures Ministry of Education, Southeast University, Nanjing 210096, China. Email: xinwang@seu.edu.cn.

Zhishen Wu, Key Laboratory of C & PC Structures Ministry of Education, Southeast University, Nanjing 210096, China. Email: zhishenwu@seu.edu.cn.

Essam Jnead, School of Civil, Mining, and Environmental Engineering, University of Wollongong, Wollongong, NSW 2522, Australia. Email: essam@unitedcrib.com.au.

How to cite this article: Ali YMS, Wang X, Wu Z, Jnead E. Flexural performance and design assessment of sustainable crumb rubber concrete beams reinforced with basalt-FRP bars. Structural Concrete. 2026. https://doi.org/10.1002/suco.70697